

УДК 530.14

QUADRUPOLE OSCILLATIONS AS PARADIGM OF THE CHAOTIC MOTION IN NUCLEI

*V. P. Berezovoj, Yu. L. Bolotin, V. Yu. Gonchar, M. Ya. Granovsky**

National Scientific Centre Kharkov Institute of Physics & Technology, Kharkov, Ukraine

INTRODUCTION. FORMULATION OF THE PROBLEM	388
REGULAR AND CHAOTIC CLASSICAL DYNAMICS OF QON	390
Hamiltonian-Scaling Properties and Geometry of Potential En- ergy Surface.	390
Critical Energy of Transition to Chaos.	394
Regularity-Chaos-Regularity Transition.	403
QUANTUM MANIFESTATIONS OF THE CLASSICAL STO- CHASTICITY	406
The Quantum Chaos Problem.	406
Numerical Procedure.	407
Quantization by the Birkhoff–Gustavson Normal Form.	411
R-C-R Transition and Statistical Properties of Energy Spec- trum of the QON.	417
R-C-R Transition and the Structure of QON Wave Function.	423
Evolution of Shell Structure in the Process of R-C-R Transi- tion.	427
Wave Packet Dynamics.	433
Chaotic Regimes in Reactions with Heavy Ions.	441
CONCLUDING REMARKS	441
REFERENCES	444

*Pro Training Tutorial Institute, 18 Stoke Av., Kew 310/4 Melbourne, Vic., Australia.

УДК 530.14

QUADRUPOLE OSCILLATIONS AS PARADIGM OF THE CHAOTIC MOTION IN NUCLEI

*V. P. Berezovoj, Yu. L. Bolotin, V. Yu. Gonchar, M. Ya. Granovsky**

National Scientific Centre Kharkov Institute of Physics & Technology, Kharkov, Ukraine

A complete description of classical dynamics, generated by the Hamiltonian of quadrupole nuclear oscillations, is presented. Those peculiarities of quantum dynamics which can be interpreted as quantum manifestations of classical stochasticity are identified. Semiclassical approximation to an energy spectrum is developed through quantization of the Birkhoff–Gustavson normal form. We show that the type of classical motion is correlated with the structure of the stationary wave functions. Correlations were found both in the coordinate space (the lattice of nodal curves and the distribution of the probability density) and in the Hilbert space associated with the integrable part of the Hamiltonian. Quadrupole oscillations of nuclei were used to investigate the shell structure destruction induced by the increase of nonintegrable perturbation which models residual nucleon–nucleon interaction. The process of wave packet tunneling through potential barrier is considered for the case of finite motion. We demonstrate that the stringent correlation between the level quasi-crossing and the wave function delocalization, which leads to the resonant tunneling, takes place.

Представлено полное описание классической динамики, генерируемой гамильтонианом квадрупольных колебаний ядер, и идентифицированы те особенности квантовой динамики, которые можно интерпретировать как квантовое проявление классической стохастичности. С помощью квантования нормальной формы Биркгофа–Густавсона получено квазиклассическое приближение для энергетического спектра. Показано, что тип классического движения коррелирует со структурой стационарных волновых функций. Корреляции обнаружены как в координатном пространстве (решетка узловых линий и распределение плотности вероятности), так и в гильбертовом пространстве, связанном с интегрируемой частью рассматриваемого гамильтониана. Квадрупольные осцилляции ядер были использованы для изучения разрушения оболочечной структуры по мере увеличения неинтегрируемого возмущения, моделирующего остаточное нуклон–нуклонное взаимодействие. Показано, что имеющие место жесткие корреляции между квазипересечением уровней и делокализацией волновой функции приводят к резонансному туннелированию.

1. INTRODUCTION. FORMULATION OF THE PROBLEM

Quite often in different areas of physics statistical properties are introduced by means of postulates or hypotheses that are self-justified only within some limiting case. Such an approach a priori suggests an existence of a mechanism of randomness, the nature of which is rooted usually outside the theory under

*Pro Training Tutorial Institute, 18 Stoke Av., Kew 310/4 Melbourne, Vic., Australia.

discussion. Results obtained in the thermodynamic limit for systems with a small number of degrees of freedom look at least questionable. Currently, however, one can consider as a rigorously established fact an existence of such dynamical systems with a small number of degrees of freedom for which under certain conditions classical motion could not be distinguished from random motion [1–9]. Typical features of these systems are nonlinearity and absence of an external source of randomness. Thus, using such synonyms for the term «random» as «chaotic», «stochastic», «irregular», one can state that there are systems with finite number of degrees of freedom, for which these notions express adequately internal fundamental properties that comprise an important and interesting subject for investigation. For the last 30–40 years we excruciatingly came to understanding that the random motion for the systems with more than one degree of freedom is almost so much customary as regular motion is. Instances of a chaotic motion, number of which permanently continues to grow, have been detected practically in every field of [1–9].

The current rebirth of interest to the nuclear dynamics resulted from the recent progress in understanding of the chaotic aspects of nonlinear dynamics systems. By reason of the richness of experimental data and sufficient precision of the theory, the nuclear dynamics provides useful realistic model for studying classical chaos and quantum manifestations of the classical stochasticity.

Conception of chaos has been introduced in the nuclear theory within the last twenty years [7–22]. This conception brought birth to the new notion in the nuclear structure [10, 13, 14, 16, 23], nuclear reactions [11, 15, 22], it could resolve a sequence of the very old contradictions in the nuclear theory [16, 24]. A radically new universal approach to the problem of statistical properties of the energy spectra was developed on the basis of the general nonlinear theory of dynamical systems [25]. Considerable advances have been made in the area of concrete nuclear effects: single particle in a deformed potential [13], nuclear fission [12], Ericson's fluctuations [26], dynamics of the 3α -linear chain [27], transition order-chaos-order in the roto-vibrational nuclear model [28, 29], chaotic scattering of α -clustering nuclei [30], concept of nuclear friction [31]. Finally, straightforward observations of the chaotic regimes in the course of simulations of the heavy-ion reactions [11] verify in favor of the general considerations.

According to Baranger [18], there are two possible chaotic philosophies in nuclear physics:

Philosophy 1. Nuclei are complicated, and chaos comes out of this complication. We expect to find chaos almost everywhere in nuclear physics. The interesting information is contained in those few places in which chaos is absent. We must look for nonchaos.

Philosophy 2. Chaos is a property of simple systems; otherwise it's no fun at all. The interesting new information is to be found in those simple areas of

nuclear physics which we used to think we could understand, but which turn out to be chaotic. We must look for chaos.

The basis of the present report is the simple chaos philosophy — Philosophy 2. Within the limits of this philosophy a general investigation of nonlinear dynamical system involves the following steps.

1. Investigation of classical phase space in order to detect chaotic regimes; numerical investigation of the classical equation of motion.
2. Analytical estimation of the critical energy for the onset of global stochasticity.
3. Test for quantum manifestations of classical stochasticity (QMCS) in the energy spectra, eigenfunctions and wave packet dynamics.
4. Consideration of interrelationship between stochastic dynamics and concrete physical effects.

The basic subject matter of the current report is to realize at least partially the outlined program for the large-amplitude quadrupole oscillation of nuclei (QON). Classical (regular and chaotic) dynamics of QON was investigated in detail in our previous review [17]. In our present work, not to burden the reader unduly, we will touch on this subject very shortly. We will pay our attention strictly to identification of only those peculiarities of quantum dynamics, which can be interpreted as the QMCS. For this purpose following problems will be discussed further:

- 1) the Birkhoff's–Gustavson's quantum normal forms;
- 2) the change of the statistical properties of the energy spectra in regularity-chaos-regularity (R-C-R) transition;
- 3) the change of the structure of wave functions in R-C-R transition;
- 4) the destruction and the reconstruction of the shell structure in R-C-R transition;
- 5) the dynamics of wave packets.

Finally some words in concern to the categories of readers whom this report is counted on. First, we would like to concentrate the attention of experts in all areas of chaos to stretch out perspective field of application of general theory of nonlinear dynamical systems. Second, we would like to persuade nuclear experts that philosophy of simple chaos could be as much useful as traditional statistical approaches are.

2. REGULAR AND CHAOTIC CLASSICAL DYNAMICS OF QON

2.1. Hamiltonian-Scaling Properties and Geometry of Potential Energy Surface. It can be shown [32] that using only the transformation properties of the interaction, the deformational potential of surface quadrupole oscillations of

nuclei takes on the form

$$U(a_0, a_2) = \sum_{m,n} C_{mn} (a_0^2 + 2a_2^2)^m a_0^n (6a_2^2 - a_0^2)^n, \quad (2.1)$$

where a_0 and a_2 are internal coordinates of nuclear surface during the quadrupole oscillations

$$R(\theta, \varphi) = R_0 \{1 + a_0 Y_{2,0}(\theta, \varphi) + a_2 [Y_{2,2}(\theta, \varphi) + Y_{2,-2}(\theta, \varphi)]\}. \quad (2.2)$$

Constants C_{mn} can be considered as phenomenological parameters, which within the limits of the particular models or approximations (for instance, ATDHF theory) can be directly related to the effective interaction of the nucleons in nucleus [33]. While in the construction of (2.1) only transformation properties of interaction are used, this expression describes potential energy of quadrupole oscillations of a liquid drop of any nature.

Restricting ourselves with the members of the fourth degree in the deformation, and assuming the equality of mass parameters for two independent directions, we get the following C_{3v} -symmetric Hamiltonian

$$H = \frac{p_x^2 + p_y^2}{2m} + U(x, y; a, b, c), \quad (2.3)$$

where

$$U(x, y; a, b, c) = \frac{a}{2} (x^2 + y^2) + b \left(x^2 y - \frac{1}{3} y^3 \right) + c (x^2 + y^2)^2, \quad (2.3a)$$

$$x = \sqrt{2} a_2, \quad y = a_0, \quad \frac{a}{2} = C_{10}, \quad b = 3C_{01}, \quad c = C_{20}.$$

C_{3v} symmetry of potential surface becomes obvious in polar coordinates

$$x = \beta \sin \gamma, \quad y = \beta \cos \gamma, \quad (2.4)$$

where β is the so-called parameter of deformation of axial symmetric nucleus, and γ is the parameter of nonaxiality. In these coordinates

$$U(\beta, \gamma; a, b, c) = \frac{1}{2} a \beta^2 - \frac{1}{3} b \beta^3 \cos 3\gamma + c \beta^4. \quad (2.5)$$

There are three possibilities of introduction of the typical unit of length l_{0i} ($i = 1, 2, 3$) for the Hamiltonian (2.3):

1) as the distance l_{01} , where the contributions from harmonic and cubic terms become comparable;

2) as the distance l_{02} , where the contributions from harmonic and biquadratic terms become comparable;

3) as the distance l_{03} , where the contributions from cubic and biquadratic terms become comparable.

Scaling of the principal physical values

$$(x, y) = l_{0i}(\bar{x}, \bar{y}), \quad (p_x, p_y) = p_{0i}(\bar{p}_x, \bar{p}_y), \quad E = \varepsilon_{0i}\bar{E} \quad (2.6)$$

for these three cases is determined by the following parameters

$$\begin{aligned} l_{01} = \frac{a}{b}, \quad p_{01} = \sqrt{m\frac{a^3}{b^2}}, \quad \varepsilon_{01} = \frac{a^3}{b^2}, \quad l_{02} = \sqrt{\frac{a}{c}}, \quad p_{02} = \sqrt{m\frac{a^2}{c}}, \\ \varepsilon_{02} = \frac{a^2}{c}, \quad l_{03} = \frac{b}{c}, \quad p_{03} = \sqrt{m\frac{b^4}{c^3}}, \quad \varepsilon_{03} = \frac{b^4}{c^3}. \end{aligned} \quad (2.7)$$

The reduced Hamiltonian for these three variants of scaling is the following

$$\bar{H}_i(\bar{p}_x, \bar{p}_y, \bar{x}, \bar{y}; W \equiv \frac{b^2}{ac}) = \frac{\bar{p}_x^2 + \bar{p}_y^2}{2} + \bar{U}_i(\bar{x}, \bar{y}, W), \quad (2.8)$$

where

$$\begin{aligned} \bar{U}_1(\bar{x}, \bar{y}; W) &= \frac{1}{2}(\bar{x}^2 + \bar{y}^2) + \left(\bar{x}^2\bar{y} - \frac{1}{3}\bar{y}^3\right) + \frac{1}{W}(\bar{x}^2 + \bar{y}^2)^2, \\ \bar{U}_2(\bar{x}, \bar{y}; W) &= \frac{1}{2}(\bar{x}^2 + \bar{y}^2) + \sqrt{W}\left(\bar{x}^2\bar{y} - \frac{1}{3}\bar{y}^3\right) + (\bar{x}^2 + \bar{y}^2)^2, \\ \bar{U}_3(\bar{x}, \bar{y}; W) &= \frac{1}{2W}(\bar{x}^2 + \bar{y}^2) + \left(\bar{x}^2\bar{y} - \frac{1}{3}\bar{y}^3\right) + (\bar{x}^2 + \bar{y}^2)^2. \end{aligned} \quad (2.9)$$

The transition $i \rightarrow k$ between the different variants of scaling is realized with the help of the substitution

$$(\bar{x}, \bar{y}) \rightarrow (\bar{x}, \bar{y}) \frac{l_{0k}}{l_{0i}}, \quad (\bar{p}_x, \bar{p}_y) \rightarrow (\bar{p}_x, \bar{p}_y) \frac{p_{0k}}{p_{0i}}, \quad \bar{E} = \frac{\varepsilon_{0k}}{\varepsilon_{0i}}\bar{E}. \quad (2.10)$$

At any variant of scaling, the reduced Hamiltonian depends only on parameter W . This is the unique dimensionless parameter, which can be constructed from the dimensional values a, b, c . It means that for each trajectory of «physical» Hamiltonian (2.3) with energy E , there corresponds the unique trajectory of one-parameter Hamiltonian (2.8) with energy $\bar{E} = E/\varepsilon_{0i}$. While for each trajectory of the reduced Hamiltonian $\bar{H}_i(W)$ with energy \bar{E} , there corresponds the whole set of «physical» trajectories with energy $E = \varepsilon_{0i}\bar{E}$, which are generated by Hamiltonians $H(a, b, c)$ with parameters that must satisfy the following condition $b^2/ac = W$.

Now, let's investigate the geometry of two-dimensional set of potential functions $U(x, y; W)$. The set of solutions of the system of equations

$$U'_x = 0, \quad U'_y = 0, \quad \det \hat{S} = 0, \quad (2.11)$$

where \hat{S} is the matrix of stability

$$\hat{S} = \begin{pmatrix} U''_{xx} & U''_{xy} \\ U''_{xy} & U''_{yy} \end{pmatrix}, \quad (2.12)$$

serves as the separatrix in the space of the parameters and divides it into the regions, where the potential function is structurally stable. The number and the nature of critical points change at the transition through separatrix $W = 16$ and under the change of sign W (i.e., under the change of sign a ; c is always positive). The critical points of PES for each structurally stable regions are given in Table 1.

Table 1. Number of critical points for different W

	Range	Critical points	Saddles	Minima	Maxima
I	$0 < W < 16$	1	0	1	0
II	$W > 16$	7	3	4	0
III	$W < 0$	7	3	3	1

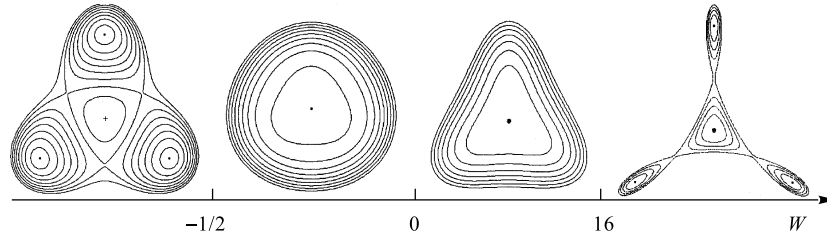


Fig. 1. The level lines of the PES for different structurally stable regions

Corresponding potential level lines are represented in Fig. 1. Coordinates of critical points are determined by

$$\begin{aligned} \bar{x}_1 = 0, \quad y_1 = 0; \quad \bar{x}_{2,3} = 0, \quad y_{2,3} = \frac{\alpha_i}{8} \left(1 \pm \sqrt{1 - \frac{16}{W}} \right), \\ x_{4-7} = \pm \sqrt{3} y_{4-7}, \quad y_{4-7} = -\frac{\alpha_i}{16} \left(1 \pm \sqrt{1 - \frac{16}{W}} \right), \end{aligned} \quad (2.13)$$

where $\alpha_1 = W, \alpha_2 = \sqrt{W}, \alpha_3 = 1$.

The region of the space of parameters $0 < W < 16$ includes potentials possessing the unique extremum — the minimum in the origin of coordinates, that corresponds to the spherically symmetric equilibrium shape of nucleus. The region $W > 16$ includes potential surfaces with four minima. The central minimum, with $x = y = 0$, corresponds to the spherically symmetric equilibrium shape of nucleus, whereas three peripheral minima correspond to the deformed shape. Finally in the region $W < 0$ ($a < 0$), we run into the potentials, describing the nuclei, which are deformed in the ground state and even don't have the quasistable spherically symmetric excited state.

2.2. Critical Energy of Transition to Chaos. If we used the term stochastization in reference to the process of appearance in the system of statistical properties in consequence of local instability, we obtain an attractive offer of identifying the values of parameters, that lead to the local instability in the system, with the boundary of transition to chaos. Unfortunately, the criteria of the stochasticity of the similar type posses the innate lack: the lost of stability of the regular motion does not obligatory leads to chaos. Whereas the transition to more complicated type of regular motion is possible. Nevertheless, the statement, that the local instabilities define the global dynamics of the system, is disputed. Separate details of the derivation of the concrete criteria of the stochasticity provoke several objections. In spite of these serious lacks, the available experience allows us to state, that the criteria of the similar type in the aggregate with numerical experiment essentially facilitate the analysis of the many-dimensional nonlinear motion.

2.2.1. Negative Curvature Criterion. A large variety of criteria of the stochasticity is based on the direct evaluation of the rate of divergence of the initially close trajectories $\{\mathbf{q}_1(t), \mathbf{p}_1(t)\}$ and $\{\mathbf{q}_2(t), \mathbf{p}_2(t)\}$. Linearized equation of motion for a divergence

$$\xi(t) = \mathbf{q}_1(t) - \mathbf{q}_2(t), \quad \eta(t) = \mathbf{p}_1(t) - \mathbf{p}_2(t) \quad (2.14)$$

assumes the following form

$$\dot{\xi}(t) = \eta, \quad \dot{\eta}(t) = \hat{S}(t)\xi, \quad (2.15)$$

where $\hat{S}(t)$ is a matrix of stability (2.12) calculated along the support trajectory $\mathbf{q}_1(t)$.

The stability of motion of the dynamic system, described by the Hamiltonian

$$H(\mathbf{p}, \mathbf{q}) = \frac{\mathbf{p}^2}{2} + U(\mathbf{q}), \quad (2.16)$$

is determined in N -dimensional case by $2N \times 2N$ matrix

$$\hat{\Gamma} = \begin{vmatrix} \hat{O} & \hat{I} \\ -\hat{S}(t) & \hat{O} \end{vmatrix}, \quad (2.17)$$

where \hat{O} and \hat{I} are a zero and a unit $N \times N$ matrices. If even one of the eigenvalues λ_i of the matrix $\hat{\Gamma}$ is real, then the divergence of the trajectory increases exponentially and the motion is unstable. The imaginary eigenvalues correspond to the stable motion. The eigenvalues and the character of motion change with time.

The problem of the investigation of the stable motion can be simplified [34] if we assume the possibility of the replacement $\mathbf{q}(t)$ by time-independent coordinate \mathbf{q} . It reduces the equations for variations (2.15) to a system of autonomous linear differential equations

$$\dot{\xi} = \eta, \quad \dot{\eta} = \hat{S}(\mathbf{q})\xi. \quad (2.18)$$

An equation for Lyapunov exponents λ_i , which determine the character of motion

$$\left| \det \hat{\Gamma} - \lambda \hat{I} \right| = 0 \quad (2.19)$$

for the system with two degrees of freedom (the system of our interest) has the following solution

$$\lambda_{1,2,3,4} = \pm \left[-\beta \pm \sqrt{\beta^2 - 4\gamma} \right], \quad (2.20)$$

where

$$\beta = \text{Sp } \hat{S} = U_{xx} + U_{yy}, \quad \gamma = \det \hat{S} = U_{xx} U_{yy} - U_{xy}^2. \quad (2.21)$$

We will assume that $\beta > 0$. Provided that $\gamma > 0$, Lyapunov exponents are purely imaginary and the motion is stable. With $\gamma < 0$, the pair of roots becomes real and it leads to exponential divergence of the trajectories, i. e., to the instability of motion.

Now let's remind several known facts from the theory of surfaces [35]. Gaussian curvature of a surface is equal to the ratio of the determinants of the second \hat{b} and the first \hat{g} quadratic forms

$$K = \frac{b_{11}b_{22} - b_{12}^2}{g_{11}g_{22} - g_{12}^2} = \frac{\det \hat{b}}{\det \hat{g}}. \quad (2.22)$$

In particular, if the surface is given in the form of the graph $z = U(x, y)$, then

$$\det \hat{b} = \frac{U''_{xx}U''_{yy} - (U''_{xy})^2}{1 + (U'_x)^2 + (U'_y)^2}, \quad \det \hat{g} = 1 + (U'_x)^2 + (U'_y)^2 \quad (2.23)$$

and therefore

$$K(x, y) = \frac{(U''_{xx})(U''_{yy}) - (U''_{xy})^2}{(1 + (U'_x)^2 + (U'_y)^2)^2}. \quad (2.24)$$

Recently, in different sections of physics, a definite interest has grown to the surfaces which everywhere possess a negative curvature [36]. Such surfaces in the neighbourhood of any point behave as in the neighbourhood of the hyperbolic singular point. Now let's return to the expression of Lyapunov exponents in the case of two-dimensional potential surfaces. Comparing the (2.21) and (2.24) expressions we notice that the sign of γ coincides with the sign of Gaussian curvature of the PES. This association suggests [37, 38] the possibility of the existence of the following scenario of the transition from regular to chaotic motion, based on the investigation of Gaussian curvature of the PES.

At low energies the motion near the minimum of the potential energy, where the curvature is obviously positive, is periodic or quasiperiodic in character and is separated from the instability region by the zero curvature line. As the energy grows, the «particle» will stay for some time in the negative curvature region of the PES where initially close trajectories exponentially diverge. At large time, these results in the motion, which imitates a random one and is usually called stochastic. According to this stochastization scenario, the critical energy of the transition to chaos, E_{cr} , coincides with the lowest energy on the zero curvature line

$$E_{cr} = U_{\min}(K = 0). \quad (2.25)$$

In the subsequent discussion we will refer to this statement, as to the negative curvature criterion (NCC).

2.2.2. Overlap Resonance's Criterion. Now we shall concentrate our attention on one of the first, widely used criterion of transition to chaos, the so-called overlap resonance's criterion (ORC) [39]. The essence of this criterion is easier to explain by the example of one-dimensional Hamiltonian system, which is subjected to periodic perturbation. This one is the simplest Hamiltonian system, which assumes the chaotic behaviour

$$H = H_0(p, x) + Fx \cos \Omega t. \quad (2.26)$$

For unperturbed system we can always introduce the variables action-angle (I, θ) in which

$$H = H_0(I) + \sum_{k=-\infty}^{\infty} x_k(I) \cos(k\theta - \Omega t), \quad (2.27)$$

where

$$x_k(I) = \frac{1}{2\pi} \int_0^{2\pi} d\theta e^{ik\theta} x(I, \theta). \quad (2.28)$$

In new variables, the scenario of stochasticity, on which ORC is based, is the following. An external periodic in time field induces a dense set of resonances in the phase space of a nonlinear conservative Hamiltonian system. The positions of these resonances, I_k are determined by the resonance condition between the eigenfrequency $\omega(I) = \frac{\partial H_0}{\partial I}$ and frequency of the external perturbation, Ω . For very weak external fields, the principle resonance zones remain isolated. As the amplitude F of external field is raised, the widths W_k of the resonance zones increase

$$W_k = 4 \left(\frac{F x_k}{\omega'(I)} \right)^{1/2} \Big|_{I=I_k} \quad (2.29)$$

and at $F > F_{\text{cr}}$ resonances overlap. When this overlap occurs, i. e., under the condition

$$\frac{1}{2} (W_k + W_{k+1}) = |I_k - I_{k+1}| \quad (2.30)$$

it is said that there is a transition to a global stochastic behaviour in the corresponding region of the phase space. The averaged motion of the system in the neighbourhood of the nonlinear isolated resonance on the plane of the variables action-angle is similar to the particle behavior in the potential well. Isolated resonances correspond to isolated potential wells. The overlap of the resonances means, that there is such an approach of the potential wells, wherein the random walk of a particle between these wells is possible.

The outlined scenario can easily be «corrected» for the description of the transition to chaos in the conservative system with several degrees of freedom. The condition of the resonance between the eigenfrequency and the frequency of external field must be replaced by the condition of the resonance between the frequencies, which correspond to different degrees of freedom

$$\sum m_i \frac{\partial H_0}{\partial I_i} = 0. \quad (2.31)$$

The role of the amplitude of external field in this case plays the intensity of the interaction between different degrees of freedom, i. e., the measure of nonlinearity of the original Hamiltonian.

This method must be slightly modified for the systems with the unique resonance. In this case the origin of the large-scale stochasticity is connected [40] with the destruction of the stochastic layer near the separatrix of this unique resonance. The essence of the modification consists in the approximate reduction of the original Hamiltonian in the neighbourhood of resonance to the Hamiltonian of nonlinear pendulum, which interacts with periodic perturbation.

2.2.3. Numerical Results versus Analytical Estimations. Now let us turn to the analysis of the solutions of the equations of motion, which are generated by the Hamiltonian (2.3). As mentioned above in Sec.2.1, the geometry of the PES for the regions I) $0 < W < 16$; II) $W > 16$; III) $W < 0$ ($a > 0$) is essentially different. Undoubtedly the specific character of the PES must be manifested in behaviour of the solutions of the equations of motion. Therefore we

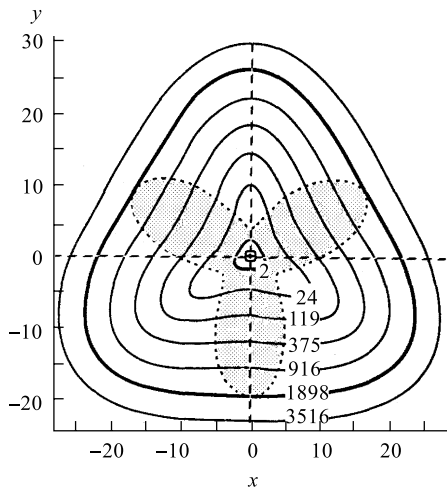


Fig. 2. Isolines of the PES for $W = 13$ and zero curvature line $K(x, y) = 0$ (dashed line); the range $K(x, y) < 0$ is shaded

shall analyse each of the mentioned regions separately. Notice, that parameters of the Hamiltonian a, b, c were estimated in different phenomenological models [41]. They change in such wide limits that for real nuclei parameter $W = b^2/ac$ can belong to each of the regions I, II, III.

Region $0 < W < 16$: Potentials with Unique Extremum. It is the simplest region for the analysis in which agreement between the boundary of the transition to chaos, observed in numerical experiments and analytical evaluations, can be obtained with the help of the simplest of the criterion of the transition to chaos-NCC. Let's remind, that according to this criterion, critical energy of the transition to chaos coincides with the minimum

$$\frac{1}{48W^2} - \frac{W-4}{12W}(\bar{x}^2 + \bar{y}^2) - \left(\bar{x}^2\bar{y} - \frac{1}{3}\bar{y}^3\right) = 0, \quad (2.32)$$

and potential energy on the zero curvature line is

$$U^{K=0}(\bar{x}, \bar{y}) = \frac{1}{48W^2} - \frac{W-10}{12W}(\bar{x}^2 + \bar{y}^2) + 2(\bar{x}^2 + \bar{y}^2)^2. \quad (2.33)$$

As is seen, the zero curvature line conserves the symmetry of the PES (see Fig.2). Therefore, the minimum of the energy on the zero curvature line must lie either on the straight line $x = 0$ or on the straight lines, obtained from it with the help of the transformations of the symmetry of the discrete group $C_{3\nu}$.

At $0 < W < 4$, Gaussian curvature of the PES is positive everywhere. At $4 < W < 12$, the subregion of the negative curvature is localized on the straight

line (in the plane) $x = 0$ in the interval

$$-\frac{1}{4} \left(1 + \sqrt{1 - \frac{4}{W}} \right) < \bar{y} < -\frac{1}{4} \left(1 - \sqrt{1 - \frac{4}{W}} \right), \quad (2.34)$$

and in the subregion $12 < W < 16$ the negative curvature appears at $\bar{y} > 0$ in the interval

$$\frac{1}{12} \left(1 - \sqrt{1 - \frac{12}{W}} \right) < \bar{y} < \frac{1}{12} \left(1 + \sqrt{1 - \frac{12}{W}} \right). \quad (2.35)$$

In Fig. 3, the profiles $U(\bar{x} = 0, \bar{y})$ of the PES are shown for the three considered subregions, and the intervals of the negative curvature are shaded.

Thus, according to the considered scenario of the stochastization in the subregion $0 < W < 4$, the motion must remain regular for all energies. According to the (2.27) in the neighbourhood of the energy

$$E_{cr} = U_{\min}(K = 0) = U \left(x = 0, y_{cr1} = -\frac{1}{4} \left(1 - \sqrt{1 - \frac{4}{W}} \right) \right), \quad (2.36)$$

the transition to the global stochasticity should be expected in the subregion $4 < W < 12$. Finally, in the subregion $12 < W < 16$, this transition must be observed in the neighbourhood of the energy

$$E_{cr} = U_{\min}(K = 0) = U \left(x = 0, y_{cr2} = \frac{1}{12} \left(1 - \sqrt{1 - \frac{12}{W}} \right) \right). \quad (2.37)$$

In this case we have used that for all $12 < W < 16$ $U(x = 0, y_{cr1}) > U(x = 0, y_{cr2})$.

These predictions must be compared with the numerical solutions of the equations of motion generated by the Hamiltonian (2.8).

The simplest numerical method of the detection of stochasticity is the analysis of the Poincare surfaces of section (PSS). The analysis of PSS, obtained by the numerical integration of Hamiltonian equations of motion, leads to the following results:

1) At low energies ($E \ll E_{cr}$) in the neighbourhood of minimum for all considered values W , the motion remains regular. The regularity of the motion with low energies is a straight consequence of the KAM theorem [42, 43], which states that the majority of the regular trajectories of the unperturbed systems remain regular under sufficiently small perturbation. It is clear that this is in accordance with the positiveness of the Gaussian curvature in the neighbourhood of any minimum.

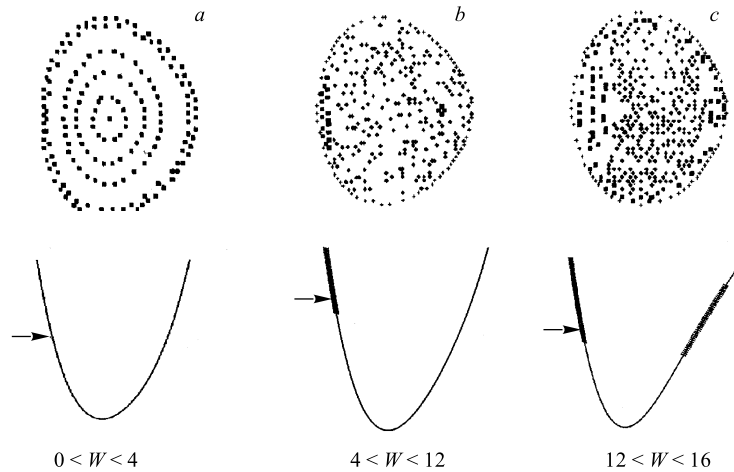


Fig. 3. The profiles $U(x=0, y)$ of the PES for $0 < W < 4$ (a), $4 < W < 12$ (b) and $12 < W < 16$ (c). The regions of the negative curvature are shaded. In the top part, the PSS for the energy values indicated by arrows, are represented

2) In the interval $0 < W < 4$ for all energies the motion remains regular (see Fig. 3, a). This can be explained by the positiveness of the Gaussian curvature of the PES in this region.

3) In the interval $4 < W < 16$ as the energy increases, the gradual transition from the regular motion to chaotic one (see Fig. 3, b) is observed. Moreover in the subregion $4 < W < 12$, the critical energy, observed in the PSS, is close to (2.38); whereas in the subregion $12 < W < 16$ the transition to the global stochasticity is observed in the neighbourhood of the energy, calculated according to (2.39). This effect at $12 < W < 16$ is connected with the beginning of the region of negative curvature at $y > 0$ located below in the energy (see Fig. 3, c).

It is necessary to make one important remark. Analysis of the PSS allows one to introduce the critical energy of the transition to chaos, determined as the energy such that part of phase space with chaotic motion exceeds certain arbitrary chosen value. Similar indetermination is connected with the absence of the sharp transition to chaos for any critical value of the perturbation. Therefore a certain caution is required for comparison of the «approximate» critical energy, obtained by numerical simulation, with the «exact» value, obtained with the help of analytical estimations, i. e., on the base of different criteria of stochasticity.

In connection with this remark we can say, that in the case of one-well potentials, the NCC allows one to make reliable predictions relative to the possibility of the existence of chaotic regimes in the considered region of the parameters; as

well as to evaluate the region of energies at which the transition regularity-chaos (R-C) is performed.

Region $W > 16$: Potentials with a Few Local Minima. Consider next numerical solutions of the equations of motion in region $W > 16$. The more complicated geometry of the PES assumes the existence of several energies of the transition to chaos even for the fixed set of parameters of the potential. It means, that for such potentials the so-called mixed states [44] must be observed: at one and the same energy in different minima the various dynamic regimes are

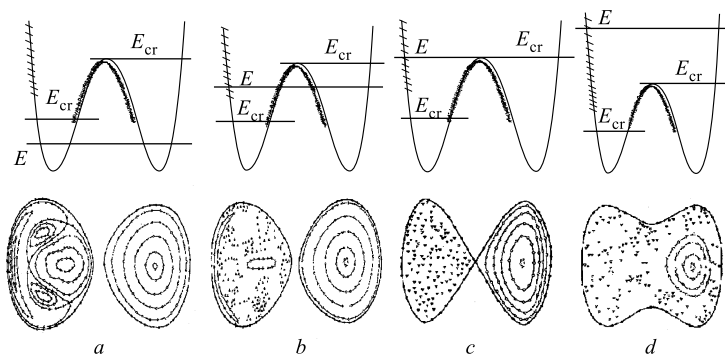


Fig. 4. The PSS for the motion in the potential with $W = 18$ at different energies: a) $E \ll E_{cr}$; b) $E > E_{cr}$; c) $E = E_S$; d) $E > E_S$. The profile $U(x = 0, y)$ of potential is presented below. The range of $K < 0$ is shaded

realized. The PSS at different energies for Hamiltonian (2.8) with $W = 18$ are presented in Fig. 4. This value W provides equality of depths for the central and peripheral minima. Taking into account C_{3v} symmetry of the PES, only one peripheral minimum is presented.

The motion represented in Fig. 4, a has clearly defined quasiperiodic character both for the central (left minimum) and for the peripheral (right) minima. Special attention must be given to the distinction in the structure of the PSS for different minima: the complicated structure with several fixed points in left minimum and simple structure with the unique fixed elliptic point in right one. The gradual transition to chaos is observed with the increasing of energy, however the change of the character of motion of the trajectories, localized in certain minimum, is essentially different. Whereas there is the gradual transition to chaos for the left well even at the energy approximately equal to one-half of the saddle energy (Fig. 4, b), and at the saddle energy (Fig. 4, c), practically all initial conditions correspond to the chaotic trajectories, the motion remains quasiperiodic in the

right minimum at the same energies. In this minimum, the transition to global stochasticity takes place only at the neighbourhood of the saddle energy. In the right well, the significant part of phase space corresponding to quasiperiodic motion

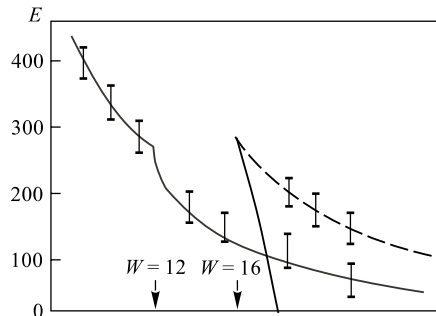


Fig. 5. The critical energy of the transition to chaos: the negative curvature criterion (rigid line) and with the help of the analysis of the Poincare section

by means of numerical integration of the equations of motion while contradicts the situation for the right well, where the numerical simulation detects large-scale chaos only at attainment of the saddle energy.

The mixed state, which is shown above for the potential of quadrupole oscillations, is the representative state for the wide class of two-dimensional potentials with a few local minima. We investigated this problem [45] by the example of the polynomial potentials of the degree not higher than six, which are symmetric relatively to the plane $x = 0$. But even with such restrictions, the possible set of the potential forms, depending (generally speaking) on 12 parameters, is too great. Remaining generality, we shall use the methods of the theory of catastrophe [44] in order to reduce the amount of calculations. According to the last one, a rather wide class of polynomial potentials with the several local minima is covered by the germs of the lowest umbilical catastrophes, of type D_5 , D_4^- , D_7 , subjected to the definite perturbations. Let us notice, that the potential of type Henon–Heiles coincides with the elliptic ombilic D_4^- [46].

The mixed state is observed for all considered potentials of umbilical catastrophes in the interval of energies $E_{cr} < E < E_S$ (E_{cr} — the critical energy of the transition to chaos determined by NCC). Transition to chaos (contrary to the NCC) is observed only at the reach of the saddle energy for the minima possessing unique fixed elliptic point in the PSS, as in the case of the potential of QON. This contradiction can be solved by the use of the ORC described in Sec.2.2.2 (see [17]).

tion conserves even at the energy essentially exceeding the saddle one (Fig. 4, *d*). Figure 5 shows a comparison of the critical energies of the transition to chaos obtained according to the NCC and with the help of the analysis of the PSS. On the base of this comparison we can do the following conclusions.

1) The mixed state is observed for considered potential for the region of energies $1/2E_S < E < E_S$ (E_S — saddle energy).

2) The critical energy, defined according to the NCC for the left well, is in good agreement with one obtained

2.3. Regularity-Chaos-Regularity Transition. Transition R-C for nonintegrable low-dimensional Hamiltonian, which is going on as the energy or the amplitude of external field increases, is a well-investigated process. The critical energy of this transition, calculated within the framework of different scenarios of stochastization, at least for potentials with the simple geometry, is in agreement with the results of numerical simulation. For the systems with localized region of instability (region of negative Gaussian curvature or region of overlap of nonlinear resonances) at further increasing of energy, one would expect the return to the regular motion. The critical energy of this new transition chaos-regularity (C-R) E_{cr2} will be determined by the top boundary of the region of instability. For the Hamiltonian of quadrupole oscillations (2.8)

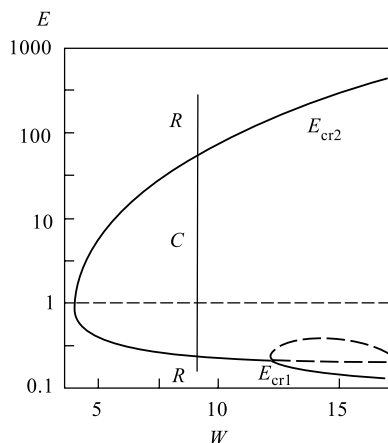


Fig. 6. The phase diagram for the R-C-R transition

$$E_{cr2} = U(x = 0, y_{cr2}), \quad y_{cr2} = -\frac{1}{4} \left(1 + \sqrt{1 - \frac{4}{W}} \right). \quad (2.38)$$

Recall that for the PES with $0 < W < 4$ at all energies the motion remains regular. Figure 6 represents the phase diagram that allows one to determine energetic intervals of regular and chaotic motions for the fixed value of W . In Fig. 7, PSS calculated for three different values of energy $E < E_{cr1}$, $E_{cr1} < E < E_{cr2}$, $E \gg E_{cr2}$ illustrate double transition (R-C-R) observable on the phase diagram (Fig. 6).

Now we would like to note the similarity in structure of phase space of considered two-dimensional autonomous Hamiltonian system with the compact region of negative Gaussian curvature and one-dimensional system with periodic perturbation.

The behavior of the width of the resonances, $\bar{W}_k \equiv 1/2(W_{k+1} + W_k)$, and the distances between them, $\Delta I_k \equiv |I_{k+1} - I_k|$, as a function of the resonance number is the simplest when the satisfaction of the resonance overlap condition (2.33) for number k_1 (at a fixed level of the external perturbation) guarantees that this condition holds for arbitrary $k > k_1$. This is precisely the situation, that prevails in the extensively studied systems of a 1D Coulomb potential [47] and a square well [48] subjected in each case to a monochromatic perturbation. In the former case we have $\bar{W}_k \approx k^{1/6}$ and $\Delta I_k \approx k^{-2/3}$, while in the latter we have $\bar{W}_k \approx k^{-1}$ and $\Delta I_k \approx [k(k+1)]^{-1}$. As can be seen from Fig. 8 there

is R-C transition (we will call this transition a «normal» transition) for both 1D Coulomb problem (*a*) and a square well (*b*), since there exists a unique point k_1 such that at $k > k_1$ the condition $\bar{W}_k > \Delta I_k$ always holds. The motion is therefore chaotic. However, as the behaviour of the widths of the resonances and of the distances between them as a function of the resonance number becomes more complex, we can allow the appearance of an additional intersection point and thus a new transition: C-R transition, which we will call «anomalous». This is also the exotic possibility of the intermittent occurrence of the regular and chaotic regions in the phase space.

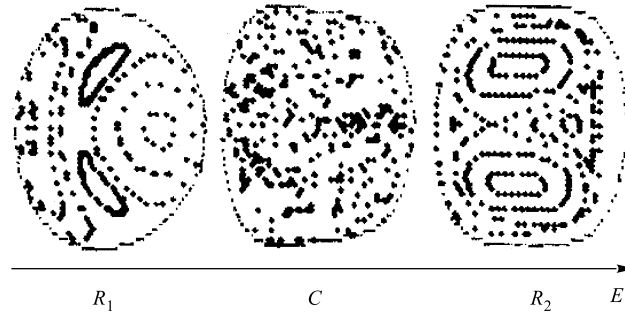


Fig. 7. PSS for three different values of energy $E < E_{cr1}$, $E_{cr1} < E < E_{cr2}$, $E \gg E_{cr2}$ illustrate the R-C-R transition observable on the phase diagram (Fig. 6)

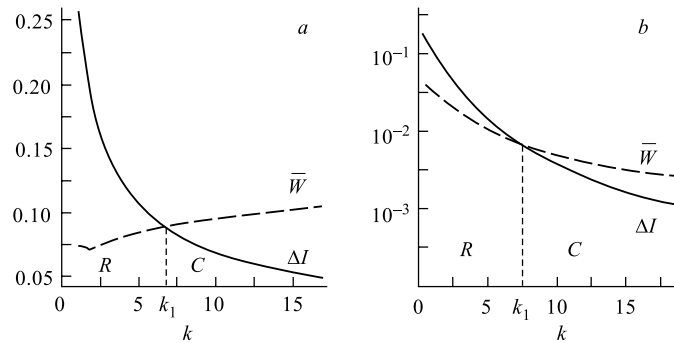


Fig. 8. The resonant spacings ΔI_k and the mean widths \bar{W}_k , as functions of the resonance number k : *a*) for one-dimensional Coulomb; *b*) for square-well potential. The critical point k_1 separates the regular range (*R*) from the chaotic one (*C*)

We demonstrate that an anomalous C-R transition occurs in a simple Hamiltonian system: an anharmonic oscillator, subjected to a monochromatic perturbation [49, 50]. The dynamics of such system is generated by the Hamiltonian

$$H(p, x, t) = H_0(p, x) + Fx \cos \Omega t, \quad (2.39)$$

where H_0 the unperturbed Hamiltonian is

$$H_0(p, x) = p^2/(2m) + Ax^n = E \quad (n = 2l, l > 1). \quad (2.40)$$

Considered system fills a gap between two extremely important physical models: the harmonic oscillator ($n = 2$) and the square well ($n = \infty$).

In terms of action-angle variables (I, q) , the Hamiltonian $H_0(p, x)$ becomes [51]

$$H_0(I) = \left(\frac{2\pi}{\alpha G(n)} I \right)^\alpha, \quad G(n) = \frac{2\sqrt{2\pi m} \Gamma(1 + 1/n)}{A^{1/n} \Gamma(1/2 + 1/n)}, \quad \alpha = \frac{2n}{n+2}. \quad (2.41)$$

The resonant values of the action I_k , that can be found from the condition $k\omega(I_k) = \Omega$, $\omega(I) = \frac{dH_0}{dI}$ are

$$I_k = \alpha \left(\frac{G(n)}{2\pi} \right)^{2n\beta} \left(\frac{\Omega}{k} \right)^{2n\alpha/\beta}, \quad \beta = \frac{1}{n-2}. \quad (2.42)$$

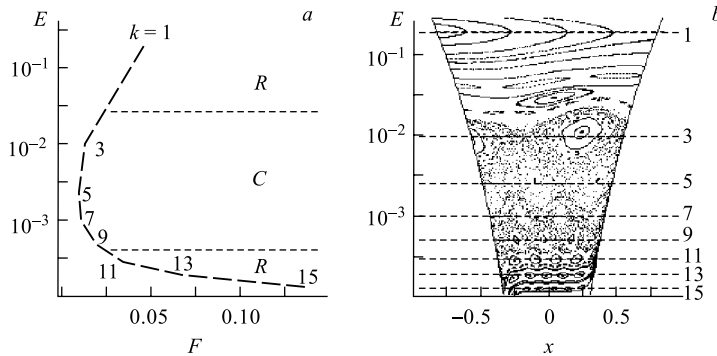


Fig. 9. *a*) The phase diagram of the R-C-R transition for Hamiltonian (2.40): the resonance energy E_k versus the critical values of the external perturbation F ($n = 8$). *b*) The snapshot of $E(x)$ confirms that the anomalous C-R transition occurs

A classical analysis, based on the ORC, leads to the following expression for the critical amplitude of the external perturbation [50],

$$F_k^{\text{cr}} = 2^{(2-3n)\beta} \frac{1}{4n} \frac{\alpha^2}{\beta} \frac{1}{x_k} \left(\frac{G(n)}{\pi} \right)^{2n\beta} \times \\ \times \Omega^{2n\beta} k^{4\beta} \left[k^{(n+2)\beta} - (k+1)^{(n+2)\beta} \right]^2, \quad (2.43)$$

where x_k is a Fourier component of the coordinate $x(I, \theta)$. Expression (2.43) solves the problem of reconstructing the structure of the phase space for arbitrary values of the parameters.

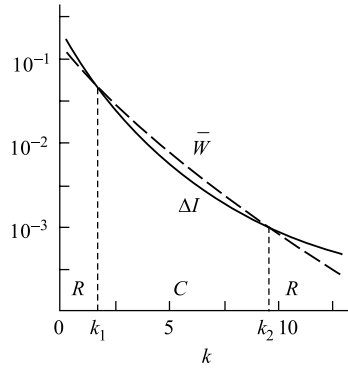


Fig. 10. The resonant spacings ΔI_k and the mean widths \bar{W}_k as functions of the resonance numbers k ($n = 8$). One can see two critical points k_1 and k_2 . The second critical point corresponds to the anomalous C-R transition

instability. In the first case this reason is a localized domain of overlap resonances, while in the second one this reason is a localized domain of the negative Gaussian curvature.

The phase diagram in Fig. 9, *a* can be used to determine, at the fixed level of the external perturbation, the energy intervals of regular and chaotic motion. The snap-shot of $E(x)$ at the right in Fig. 9, *b* confirms that an anomalous C-R transition occurs. We can clearly see isolated nonlinear resonances which persist at large values of k , and near which the motion remains regular. The reason for this anomaly is explained by Fig. 10. The plots of the resonance widths and the distances between resonances in this figure demonstrate that there are two rather than one intersection points: $k = k_1$ and $k = k_2$. Consequently, there is an anomalous C-R transition.

Thus, for 1D system with periodic perturbation R-C-R transition can be observed just as in the case of 2D autonomous Hamiltonian system. The reason of the additional transition in both cases is common: a localized region of

3. QUANTUM MANIFESTATIONS OF THE CLASSICAL STOCHASTICITY

3.1. The Quantum Chaos Problem. Essential progress in the understanding of the nonlinear dynamics of classical systems stimulated numerous attempts to include the conception of the stochasticity in quantum mechanics [1–4, 7–9,

52–55]. The essence of the problem is that the energy spectrum of any quantum system, performing the finite motion, is discrete and therefore its evolution is quasi-periodic. At the same time, the correspondence principle requires the possibility of limit transition to classical mechanics, containing not only regular solutions but also chaotic ones. The total solving of this problem is too complicated, therefore its restricted variant is of considerable interest. Our prime interest is the peculiarities of behaviour of quantum systems the classical analogies of which reveal chaotic behaviour. Such peculiarities are usually called the quantum manifestations of the classical stochasticity (QMCS). A priori the manifestations of the QMCS can be expected both in the form of some peculiarities of concrete stationary state and in the whole group of close states in energy. The following objects can be used as the objects of search of the QMCS for an autonomous systems: 1) the energy spectra; 2) the stationary wave functions; 3) the wave packets. This part of the review is dedicated to the results relating to the QMCS in the dynamics of QON.

3.2. Numerical Procedure. The quantum scaled Hamiltonian describing the quadrupole surface oscillations has the following form

$$H = \frac{\bar{\hbar}_i^2}{2}(\Delta_x + \Delta_y) + U_i(x, y, W), \quad (3.1)$$

where the scaled Planck's constant is $\bar{\hbar} = \hbar/\hbar_{0i}$, $\hbar_{0i}^2 = m\varepsilon_{0i}l_{0i}^2$, and the scaling parameters \hbar_{0i} , l_{0i} and the deformation potential $U_i(x, y, W)$ are determined by the expressions (2.7) and (2.9).

We are going to study the peculiarities of the structure of energy spectra and wave functions in each of the following intervals:

$$\begin{array}{ll} \text{the first regular region} & R_1 : 0 < E < E_{\text{cr1}}, \\ \text{the chaotic region} & C : E_{\text{cr1}} < E < E_{\text{cr2}}, \\ \text{the second regular region} & R_2 : E > E_{\text{cr2}}. \end{array}$$

The critical energies E_{cr1} and E_{cr2} were determined above. The main numerical calculations were performed for one-well potentials ($0 < W < 16$). In this case the critical energies are determined by the relations (2.36), (2.37).

At fixed topology of PES ($W = \text{const}$), the scaled Planck's constant $\bar{\hbar}_i$ is the unique free parameter in the quantum Hamiltonian (3.1). In the study of the concrete region of energies, corresponding to the certain type of classical motion (R_1, C or R_2), the choice of $\bar{\hbar}_i$ is dictated by the possibility of attainment of the required degree of validity of semiclassical approximation (large quantum numbers) at conservation of the computational precision of spectrum and wave functions (the limitation of the possibility of diagonalization of large dimension matrices). For the original nonreduced Hamiltonian (2.3) the variation of $\bar{\hbar}_i$ is equivalent to the variation of the critical energies E_{cr1} and E_{cr2} (i. e., parameters a, b, c) or to the adequate choice of Planck's constant \hbar .

The procedure of diagonalization was used for the determination of an energy spectrum and eigenfunctions [56]. As the basis we chose the simple combinations of the eigenfunctions of the two-dimensional harmonic oscillator with equal frequencies [57]

$$|NLj\rangle = \frac{P_{L,j}}{\sqrt{2}}(|NL\rangle + j|N, -L\rangle), \quad j = \pm 1, \quad (3.2)$$

$$N = 0, 1, 2 \dots; \quad L = N, N - 2 \dots 1 \text{ or } 0; \quad P_{L,j} = j^{\text{Mod}(L,3)}$$

normalized according to the condition

$$\langle NLj | N'L'j' \rangle = \frac{1}{\sqrt{2}} 2^{\delta_{L,0}} \delta_{jj'} \delta_{NN'} \delta_{LL'}. \quad (3.3)$$

The symmetry of the considered Hamiltonian C_{3v} leads to the block structure of matrix $\langle N'L'j' | H | NLj \rangle$, which consists of four independent submatrices. It allows one to carry out diagonalization of each submatrix separately, obtaining in this case four independent sets of states, which according to the classification used in the theory of groups are the following states: A_1 -type [mode $(L, 3) = 0$, $j = 1$, including $L = 0$], A_2 -type [mode $(L, 3) = 0$, $j = 1$, $L \neq 0$] and twice degenerated states E -type [mode $(L, 3) \neq 0$, $j = \pm 1$].

The possibility of separate diagonalization of submatrices of definite type allows to essentially increase available dimension of basis in numerical calculations (later for brief, we shall call the dimension of basis as the dimension n of separate submatrix). Table 2 shows the maximal oscillator numbers N_0 of the basis and the dimension m of the total matrix $\langle N'L'j' | H | NLj \rangle$ for the enumerated types of submatrices with the dimension $n = 408$.

Table 2. Maximal oscillator number N_0 of the basis and the dimensional m of submatrices $\langle N'L'j' | H | NLj \rangle$ A_1 , A_2 and $E_{1,2}$ -types

	A_1	A_2	$E_{1,2}$
N_0	67	70	48
m	2346	2556	1225

Expansion of wave eigenfunctions in the basis (3.2) in polar coordinates r, φ is

$$\langle r, \varphi | E_k \rangle = \sum_{NL} C_{NLj}^{(k)} \langle r, \varphi | NLj \rangle, \quad (3.4)$$

where

$$\langle r, \varphi | NL \rangle = i^N \frac{e^{-iL\varphi}}{\sqrt{2\pi}} \frac{1}{L!} \left[\frac{2((N+L)/2)!}{((N-L)/2)!} \right]^{1/2} \times$$

$$\times (\sqrt{\omega_0 r})^L e^{-\omega_0 r^2/2} M \left\{ -\frac{N-L}{2}, L+1, \omega_0 r^2 \right\}. \quad (3.5)$$

Here $M(\dots)$ is a degenerated hypergeometric function and ω_0 is the frequency of the oscillator basis.

The finite dimension of the basis used in calculations leads to the dependence of the position of the level on the oscillator frequency ω_0 . Such dependence for the dimensions of basis $n = 198$ and $n = 408$ ($W = 13$) is represented in Fig. 11.

The important moment of numerical calculations is the choice of the optimal frequency ω_0^{opt} , determined from the condition that the energies of levels, situated in the interval of our interest, have minimum value. Such optimization is essentially important for the regions C and R_2 where the positions of the levels depend more on the frequency of the basis. The optimal frequency depends both on the dimension of the basis and on the length of the investigated energy interval. As shown in Fig. 11 it is possible to choose the unique frequency ω_0^{opt} for intervals including decades or more levels just at the dimension of the basis $n = 408$. These levels are selected in Fig. 11 by dotted lines. The large value of ω_0^{opt} for the region R_2 ($\omega_0^{\text{opt}} \sim 8$) is caused by the fact that at energies $E > E_{\text{cr}2}$, the deformation potential essentially differs from the harmonic oscillator potential.

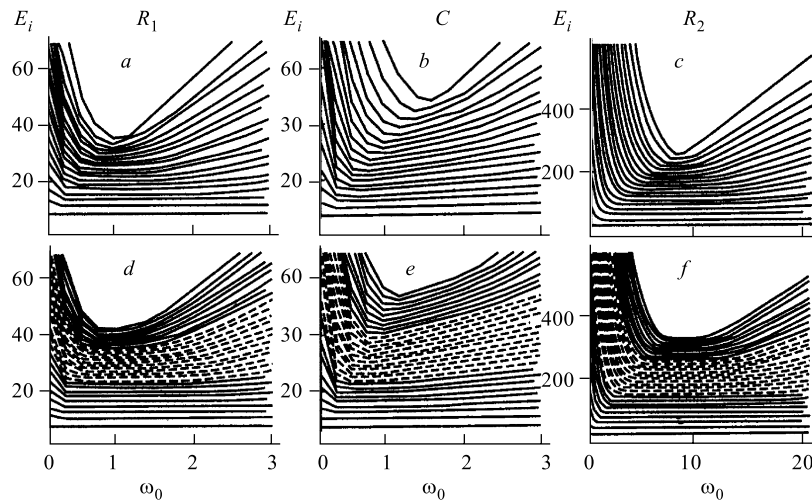


Fig. 11. Energy spectra of Hamiltonian (3.1) as a function of the frequency ω_0 of the oscillator basis ($W = 13$). The parts of this figure show this dependence for the basis dimensions $n = 198$ (a, b, c) and $n = 408$ (d, e, f), respectively

The dimension of the basis used in our calculations was determined for the reason of acceptability of the calculation time and the calculation precision of the position of levels in the considered region. The results of investigation of saturation in the basis are represented in Fig. 12. As is clear from the graph for the regions R_1 (c) and R_2 (a) acceptable precision of calculations of levels with ordinal numbers $100 \sim 200$ is reached at the dimension of the basis $n \sim 400$,

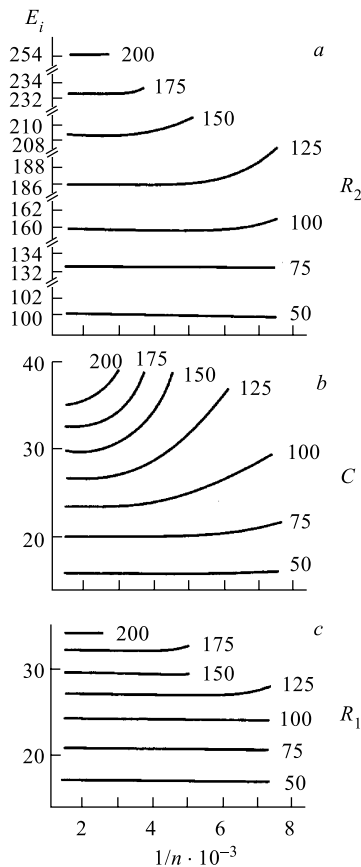


Fig. 12. Energy levels as a function of the basis dimension n . The numbers on the curves are the level numbers k

solution $\psi(\mathbf{r}, t)$ can be accurately generated with the help of the split operator FFT (Fast Fourier Transformation) method [60]. The numerical FFT of $P_1(t)$, or

while for the chaotic region C (b) the dimension of the basis requires considerably larger number ($n \sim 700$) to attain the same precision. It is a well-known result [4, 12]: the value of saturation in the basis is sensitive to the type of classical motion.

Matrix diagonalization is attractive for treating Hamiltonians that do not differ greatly from Hamiltonians with known eigenfunctions. However this numerical procedure becomes less attractive (or even not effective at all) at the transition to the PES of a complicated topology, when required Hamiltonian matrix is of high order. In this case the alternative to the diagonalization may become the so-called spectral method [58], which utilizes numerical solutions to the time-dependent Schrödinger equation. The spectral method was developed earlier for determining the eigenvalues and eigenfunctions for the modes of optical waveguides from numerical solutions of the paraxial wave equation [59]. Feit, Fleck, and Steiger [58] successfully implemented the previously developed methodology to quantum mechanical problems with a little change, as the latter equation is identical to the Schrödinger equation.

The spectral method requires the computation of the correlation function

$$P_1(t) = \langle \psi(\mathbf{r}, 0) | \psi(\mathbf{r}, t) \rangle, \quad (3.6)$$

where $\psi(\mathbf{r}, t)$ represents a numerical solution of the time-dependent Schrödinger equation, and $\psi(\mathbf{r}, 0)$ is the wave function at $t \equiv 0$. The

$P_1(E)$, displays a set of sharp local maxima for $E = E_n$, where E_n are the desired energy eigenvalues. With the aid of lineshape fitting techniques, both the positions and the heights of these resonances can be determined with high accuracy. The former yield the eigenvalues; and the latter, the weights of the stationary states that compose the wave packet once the eigenvalues are known, the corresponding eigenfunctions can be computed by numerically evaluating the integrals

$$\psi(\mathbf{r}, E_n) = \int_0^T \psi(\mathbf{r}, t) W(t) \exp(iE_n t) dt, \quad (3.7)$$

where T is the time encompassed by the calculation, and $W(t)$ is a window function,

$$W(t) = \begin{cases} 1 - \cos(2\pi t)/T, & 0 < t < T, \\ 0, & t > T. \end{cases} \quad (3.8)$$

Since the spectral method is fundamentally based on numerical solutions of a time-dependent differential equation, its implementation is always straightforward. No special ad hoc selection of the basis function is required, nor is it necessary for the potential to have a special analytic form. In principle, the spectral method is applicable to problems involving any number of dimensions.

3.3. Quantization by the Birkhoff–Gustavson Normal Form. In this section we calculate a semiclassical approximation for an energy spectrum of the Hamiltonian of QON (3.1) [17, 61, 62] (here it will be more suitable for us to use the nonscale version of the Hamiltonian (2.3) with $m = 1$) by quantization of the Birkhoff–Gustavson [63, 64] normal form (NF) and then compare the obtained results with exact quantum mechanical calculations. By the exact spectrum we mean the spectrum obtained by the direct numerical calculations, for example, by the diagonalization of the Hamiltonian on the reasonable chosen basis.

Transformation of the given Hamiltonian to a more simple form, called NF, is one of the universal methods of analyzing a classical equation of motion. This method of treating nonseparable classical systems was originally developed by Birkhoff [63] and later was extended by Gustavson [64]. The result, obtained by Birkhoff, is the following: if the given Hamiltonian H , which can be written as a formal power series without constant or linear terms, and such that the quadratic terms can be written as a sum of uncoupled harmonic oscillator terms with incommensurable frequencies, then there is a canonical transformation that transforms original Hamiltonian into NF. Last is a power series in the one-dimensional uncoupled harmonic oscillator Hamiltonian. Birkhoff's method was applied by Gustavson in order to obtain power series expressions for isolating integrals, and to predict analytically the PSS for the Henon–Helies system. Since the treated potential had commensurable frequencies, Gustavson was compelled to modify a little Birkhoff's method.

Every two-dimensional Hamiltonian near to equilibrium points can be represented in polynomial form as follows:

$$H(\mathbf{p}, \mathbf{q}) = H^{(2)}(\mathbf{p}, \mathbf{q}) + V(\mathbf{q}), \quad (3.9)$$

$$H^{(2)}(\mathbf{p}, \mathbf{q}) = \sum_{\nu} \frac{1}{2} \omega_{\nu}^2 (\mathbf{p}_{\nu}^2 + \mathbf{q}_{\nu}^2), \quad V(\mathbf{q}) = \sum_{|j| \geq 3} V_{j_1 j_2} q_1^{j_1} q_2^{j_2}, \quad (3.10)$$

$$\mathbf{q} = (q_1, q_2), \quad \mathbf{p} = (p_1, p_2).$$

The procedure of reducing to NF depends on whether the frequencies ω_{ν} of the Hamiltonian (3.9) are commensurable or not. If they are incommensurable then there exists a canonical transformation $(\mathbf{q}, \mathbf{p}) \rightarrow (\xi, \eta)$ such that in variables (ξ, η) Hamiltonian $\Gamma(\xi, \eta)$ will be a function of only two combinations $I_{\nu} = \frac{1}{2}(\xi_{\nu}^2 + \eta_{\nu}^2)$, $\nu = 1, 2, \pm$. In other words, the Birkhoff NF is an expansion of the original Hamiltonian over two one-dimensional harmonic oscillators,

$$H(\mathbf{p}, \mathbf{q}) \rightarrow \Gamma(\xi, \eta) = \omega_1 I_1 + \omega_2 I_2 + \sum \alpha_{\mu\nu} I_{\mu} I_{\nu} + \dots \quad (3.11)$$

If the frequencies ω_{ν} are commensurable, i. e., if there exist resonance relations of the type $m\omega_1 + n\omega_2 = 0$ ($m, n \in \mathbb{N} \setminus \{0\}$), the Hamiltonian (3.9) cannot be reduced to the Birkhoff NF due to the appearance of zero denominators $m\omega_1 + n\omega_2 = 0$. Therefore, one should not cancel some terms in the Hamiltonian (3.9), i. e., NF becomes more complicated and will contain apart from I_{ν} other combinations of variables ξ_{ν} and η_{ν} as well. Such an extended NF is called the Birkhoff–Gustavson NF.

The reduction of Hamiltonian to the NF solves the question about the construction of a full set of approximate integrals of motion. The latter can be found by transformation of the variables of action to initial variables. The solution of the equations

$$H(p_x, p_y, x, y) = E, \quad I(p_x, p_y, x, y) = I_0, \quad x = \text{const} \quad (3.12)$$

allows one to find the set of intersections of a phase trajectory with the selected plane ($x = \text{const}$) and by doing so to reconstruct the structure of the PSS.

The PSS for the quadrupole oscillations of nuclei ^{74}Kr , which are constructed in such a way, are shown in Fig. 13. The Hamiltonian, describing these oscillations, up to the terms of the sixth degree with respect to deformation is the following

$$H = \frac{1}{2}(p_x^2 + p_y^2) + U(x, y),$$

$$U(x, y) = \frac{a}{2}(x^2 + y^2) + b \left(x^2 y - \frac{1}{3} y^3 \right) + c(x^2 + y^2)^2 +$$

$$+ d \left(x^2 y - \frac{1}{3} y^3 \right) (x^2 + y^2) + e \left(x^2 y - \frac{1}{3} y^3 \right)^2 + f(x^2 + y^2)^3. \quad (3.13)$$

The parameters determining the dynamics of the particular nucleus, are calculated for the isotopes of Krypton in [29]. The qualitative coincidence of topology of PSS calculated with the help of NF and the numerical integration of the equations of motion is noteworthy.

Let's address now directly to the procedure of quantization. Quantization for the incommensurable case is straightforward. Since NF can be expressed entirely in terms of action variables, we merely have to replace those action variables by an appropriate multiple of \hbar , $I_\nu \rightarrow \hbar(n_\nu + 1/2)$, and the result is a power series of the quantum numbers,

$$E_{n_1 n_2} = \Gamma(n_1 + 1/2, n_2 + 1/2). \quad (3.14)$$

The commensurable case is less straightforward. Commensurability of frequencies leads to the appearance of angle variables in the normal form

$$\Gamma = \Gamma(I_1, I_2, \varphi_2). \quad (3.15)$$

As before, we can replace the action I_1 by $\hbar(n_1 + 1/2)$. In this case the initial two-dimensional problem is reduced to the one-dimensional problem, the quantization of which can be performed with the help of WKB method.

The procedure of quantization by NF will begin with the canonical transformation

$$\begin{aligned} q_1 &= \frac{i}{2}(-Q_1 + Q_2 + P_1 - P_2), & q_2 &= \frac{1}{2}(Q_1 + Q_2 + P_1 + P_2), \\ p_1 &= \frac{1}{2}(Q_1 - Q_2 + P_1 - P_2), & p_2 &= \frac{i}{2}(Q_1 - Q_2 - P_1 - P_2), \end{aligned} \quad (3.16)$$

where variables (\mathbf{p}, \mathbf{q}) provide the reduction of the harmonic part of the initial Hamiltonian (2.3) to NF,

$$H^{(2)}(\mathbf{p}, \mathbf{q}) = \sum_{k=1,2} \frac{1}{2} \omega_k (\mathbf{p}_k^2 + \mathbf{q}_k^2). \quad (3.17)$$

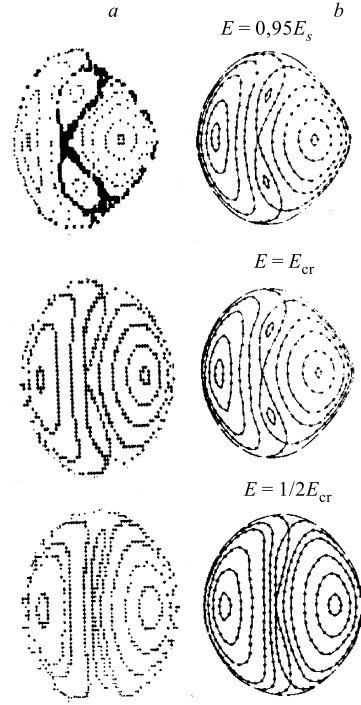


Fig. 13. The PSS for the central minimum of ^{74}Kr at different energy values: *a*) obtained by the numerical integration; *b*) obtained with the help of a normal form

In the new variables $\mathbf{Q}(Q_1, Q_2)$, $\mathbf{P}(P_1, P_2)$ the Hamiltonian of quadrupole oscillations is the following

$$K(\mathbf{Q}, \mathbf{P}) = K^{(2)}(\mathbf{Q}, \mathbf{P}) + \sum_{j>2} K^{(j)}(\mathbf{Q}, \mathbf{P}), \quad (3.18)$$

$$K^{(2)}(\mathbf{Q}, \mathbf{P}) = i(Q_1 P_1 + Q_2 P_2) \quad (3.19)$$

and $K^{(j)}$ are homogeneous polynomials in variables \mathbf{Q} and \mathbf{P} of degree j . Each member $K^{(j)}$ of the Hamiltonian (3.18) is reduced to NF according to the standard procedure [64, 17]. However this procedure is sufficiently simplified due to the diagonal form of the operator D in the variables (P, Q) . The classical NF is the sum of the polynomials of a special form in \mathbf{Q} and \mathbf{P} . For obtaining its quantum analog we can use the Weyl's heuristic rule of correspondence

$$\mathbf{P}^n \mathbf{Q}^m = \mathbf{Q}^m \mathbf{P}^n \rightarrow \frac{1}{2^n} \sum_{l=0}^n \frac{n!}{l!(n-l)!} \hat{\mathbf{Q}}^m \hat{\mathbf{P}}^{n-l}. \quad (3.20)$$

The operators $\hat{\mathbf{P}}$ and $\hat{\mathbf{Q}}$ are determined by formulae (3.16), in which by \mathbf{p} and \mathbf{q} we should mean operators of impulse and coordinate with usual rules of commutation, from which it follows that

$$[\hat{P}_k \hat{Q}_l] = \delta_{kl} \quad (k, l = 1, 2). \quad (3.21)$$

The operators $\hat{\mathbf{P}}$, $\hat{\mathbf{Q}}$ allow one to introduce the full orthonormalized basis

$$|NL\rangle = \left[\left(\frac{N+L}{2} \right)! \left(\frac{N-L}{2} \right)! \right]^{-1/2} \hat{Q}_2^{(N-L)/2} \hat{Q}_1^{(N+L)/2} |0\rangle, \quad (3.22)$$

where the vacuum state $|0\rangle$ is determined by

$$\hat{P}_1 |0\rangle = \hat{P}_2 |0\rangle = 0. \quad (3.23)$$

The principal quantum number $N = 0, 1, \dots$ and the angular momentum number L at given N is equal to $\pm N, \pm(N-2), \dots, 0$ or 1 . The action of the operators $\hat{\mathbf{Q}}$ and $\hat{\mathbf{P}}$ on the basis $|NL\rangle$ is

$$\begin{aligned} \hat{Q}_1 |NL\rangle &= \sqrt{(N+L+2)/2} |N+1, L+1\rangle, \\ \hat{P}_1 |NL\rangle &= \sqrt{(N+L)/2} |N-1, L-1\rangle, \\ \hat{Q}_2 |NL\rangle &= \sqrt{(N-L+2)/2} |N+1, L-1\rangle, \\ \hat{P}_2 |NL\rangle &= \sqrt{(N-L)/2} |N-1, L+1\rangle. \end{aligned} \quad (3.24)$$

Note that the constructed basis is oscillator one

$$\hat{K}^{(2)} |NL\rangle = (\hat{Q}_1 \hat{P}_1 + \hat{Q}_2 \hat{P}_2 \pm 1) |NL\rangle = (N + 1) |NL\rangle. \quad (3.25)$$

The classical NF for considered Hamiltonian is (through the fourth degree)

$$\begin{aligned} \Gamma = \Gamma^{(2)} + \Gamma^{(4)} = i \left[(Q_1 P_1 + Q_2 P_2) + \frac{b^2}{6} (P_1^2 Q_1^2 + P_2^2 Q_2^2 - 12 Q_1 Q_2 P_1 P_2) + \right. \\ \left. + c (P_1^2 Q_1^2 + P_2^2 Q_2^2 + 4 Q_1 Q_2 P_1 P_2) \right]. \quad (3.26) \end{aligned}$$

The quantum NF $\hat{\Gamma}$ reconstructs from the classical one with the help of Weyl's rule (3.20) and Dirac's rule of correspondence $\hat{\Gamma} \rightarrow \frac{1}{i} \Gamma$

$$\begin{aligned} \hat{\Gamma} = (\hat{Q}_1 \hat{P}_1 + \hat{Q}_2 \hat{P}_2 + 1) + \frac{b^2}{6} \left[(\hat{Q}_1 \hat{P}_1)^2 + (\hat{Q}_2 \hat{P}_2)^2 - \right. \\ \left. - 5 (\hat{Q}_1 \hat{P}_1 + \hat{Q}_2 \hat{P}_2) - 12 \hat{Q}_1 \hat{P}_1 \hat{Q}_2 \hat{P}_2 - 2 \right] + \\ + c \left[(\hat{Q}_1 \hat{P}_1)^2 + (\hat{Q}_2 \hat{P}_2)^2 + 3 (\hat{Q}_1 \hat{P}_1 + \hat{Q}_2 \hat{P}_2) + 4 \hat{Q}_1 \hat{P}_1 \hat{Q}_2 \hat{P}_2 + 2 \right]. \quad (3.27) \end{aligned}$$

It is easy to see, that basis vectors $|NL\rangle$ are eigenvectors for quantum NF (3.27). Therefore we get the simple analytical formula for the energy spectrum in the fourth approximation

$$\begin{aligned} E(N, L) = N + 1 + \frac{b^2}{12} [7L^2 - 5(N + 1)^2 + 1] + \\ + \frac{c}{2} [3(N + 1)^2 - L^2 + 1]. \quad (3.28) \end{aligned}$$

Assuming $c = 0$ in the formula (3.28) we get an approximate spectrum of the Henon–Heiles Hamiltonian, which up to the constant shift coincides with the spectra obtained by other methods. The last property, apparently, is connected with the ambiguity of quantization method of the Hamiltonian. Each level in the energy spectrum (3.22) is double degenerated with respect to sign of an angular momentum number L , whereas for the levels of the exact Hamiltonian with $L = 3k$ ($k = 1, 2, \dots$) the degeneration must be taken off. Inclusion into the NF of the members of higher degree leads to the taking off the degeneration. Really

$$\begin{aligned} \Gamma^{(6)} = \left(\frac{11}{54} b^4 + \frac{10}{9} b^2 c + 2c^2 \right) (P_1^3 Q_1^3 + P_2^3 Q_2^3) + \\ + \left(\frac{5}{12} b^4 - \frac{61}{3} b^2 c + 15c^2 \right) P_1 P_2 Q_1 Q_2 (P_1 Q_1 + P_2 Q_2) + \end{aligned}$$

$$+ \frac{2}{9} b^2 (7b^2 - 26c) (P_1^3 Q_2^3 + P_2^3 Q_1^3). \quad (3.29)$$

The last term in this relation connects the states with equal N and the states with $L' - L = \pm 6$. However in this approximation the basis vectors $|NL\rangle$ (3.22) will be no longer the eigenvectors of the NF. Therefore for the calculation of the energy spectrum it is required either additional diagonalization of the engaging states or the calculations by the theory of perturbation. How well does the energy spectrum (3.28), obtained by quantization of a classical NF in the fourth approximation, reproduce an exact quantum spectrum of the Hamiltonian of quadrupole oscillations? In Table 3, an approximate spectrum $E(NL)$ is compared with the spectrum E_{ex} , obtained by diagonalization on oscillator basis.

Table 3. Energy levels of Hamiltonian (2.3) ($b = 0.04416$, $c = 0.00015$, $E_{\text{cr}} = 90$)

	N	L	E_{approx}	E_{exact}	Type	Error $\Delta E/E$, %
1	0	0	0.9996	1.0001	A_1	0.043
2	1	1	1.9989	1.9994	E	0.022
3	2	0	2.9949	2.9954	A_1	0.015
4	2	2	2.9992	2.9996	E	0.014
5	3	1	3.9919	3.9924	E	0.012
6	3	3	4.0004	4.0008	A_1	0.010
				4.0008	A_2	0.010
7	4	0	4.9855	4.9861	A_1	0.010
8	4	2	4.9898	4.9903	E	0.010
9	4	4	5.0025	5.0059	E	0.007
10	5	1	5.9801	5.9807	E	0.010
.....						
145	23	1	23.662	23.670	E	0.032
146	23	3	23.671	23.673	A_1	0.009
				23.688	A_2	0.071
147	23	5	23.688	23.699	E	0.045
148	23	7	23.713	23.722	E	0.037
149	23	9	23.747	23.754	A_1	0.028
				23.754	A_2	0.028
150	23	11	23.790	23.794	E	0.019
.....						
246	30	10	30.541	30.558	E	0.055
247	30	12	30.588	30.601	A_2	0.043
				30.601	A_1	0.043
248	30	14	30.643	30.653	E	0.031
249	30	16	30.707	30.712	E	0.017
250	30	18	30.779	30.780	A_1	0.003
				30.780	A_2	0.003

The dimensions of submatrices of type A_1 , A_2 , E are respectively equal to 560, 560, and 415 and provide sufficient precision of calculations for the first 250–300 levels. The parameters of the Hamiltonian (2.3) are chosen so that $E_{\text{cr1}} = 90$. As can be seen from Table 3 in region, where classical motion is regular, the quantum NF reproduces the energy spectrum with the relative error $\frac{\Delta E}{E} \sim 0.01\%$. It seems natural to expect that in the neighbourhood of critical energy of the transition to chaos, where the destruction of the approximate integrals of motion takes place and with the help of which the semiclassical spectrum is built, the agreement of the last one with the exact spectrum must essentially be getting worse. We have analysed this effect by the example of a spectrum of fluctuations QON. We calculated the difference $\Delta E = E(\text{BHNF}) - E(\text{numerical})$ as the function of the energy for the case $W = 13$. The analysis shows that in the region of energies, where the classical motion is regular, the approximate spectrum (3.28) reproduces the exact one rather well. Whereas at the transition to the chaotic region the difference increases sharply. The similar situation takes place and for the Henon–Heiles Hamiltonian, too [17].

3.4. R-C-R Transition and Statistical Properties of Energy Spectrum of the QON. Important correlations between peculiarities of a classical dynamics and the structure of the quantum energy spectrum can be obtained in studies of statistical properties of level sequences. We shall be interested in local properties of the spectrum, i. e., in deviation of the distribution of levels from mean values. Why should we address to local characteristics of a spectrum? The matter is, that the global characteristics such as the numbers of states $N(E)$ or the smoothed density of levels $\rho(E)$ are too rough. At the same time, such local characteristics, as the function of the nearest-neighbour spacing distribution between levels (FNNSDL) is very sensitive to the properties of the potential and to the shape of the boundary.

Relying on rather simple reasons [65], let's try to construct one of the local characteristics of a quantum spectrum — the FNNSDL $P(S)$. For a random sequence the probability that a level will be in the small interval $(E + S, E + S + dS)$, proportional, of course, to dS , will be independent of whether or not there is a level at E . This probability will be modified if we introduce a level interaction. Given a level at E , let the probability that the next level $S \neq 0$ be in $(E + S, E + S + dS)$ be $P(S)dS$. Then for $P(S)$ we have

$$P(S)dS = P(1 \in dS | 0 \in S)P(0 \in S), \quad (3.30)$$

where $P(n \in S)$ is the probability that the interval of length S contains n levels and $P(n \in dS | m \in S)$ is the conditional probability that the interval of length dS contains n levels, when that one of length S contains m levels. The second factor in (3.30) is $\int_S^\infty P(x)dx$, the probability that the spacing is larger than S ,

while the first one will be dS times a function of S , $r_{10}(S)$, depending explicitly on the choice, 1 and 0, of the discrete variables n, m . Then

$$P(S) = r_{10}(S) \int_S^{\infty} P(x) dx \quad (3.31)$$

which we can solve easily to find

$$P(S) = c r_{10} \exp \left(- \int_0^S r_{10}(x) dx \right). \quad (3.32)$$

The Poisson law follows if we take $r_{10}(S) = 1/D$ (the absence of correlations between level positions), where D is the mean local spacing so that $1/D$ is the density of levels. Wigner's law follows from the assumption of a linear repulsion, defined by $r_{10}(S) = \alpha S$. The arbitrary constants are determined by conditions

$$\int P(x) dx = 1, \quad \int x P(x) dx = D. \quad (3.33)$$

Finally, we find for the Poisson and Wigner cases, respectively

$$P(S) = 1/D \exp(-S/D), \quad S \geq 0, \quad (3.34)$$

$$P(S) = \frac{\pi S}{2D^2} \exp \left(- \frac{\pi S^2}{4D^2} \right), \quad S \geq 0. \quad (3.35)$$

The second distribution displays the repulsion explicitly since $P(0) = 0$, in contrast to the Poisson form, which has a maximum at $S = 0$ (level clusterization).

To get a first idea about the origin of the level repulsion let us consider [65] the Hamiltonian as defined with respect to some fixed basis by its matrix elements. The repulsion may be regarded as arising from the fact that, the subspace for which the corresponding spectrum has a degeneracy, is of a dimensionality less by two than that of the general matrix-element space, so that in some sense a degeneracy is «unlikely». Alternatively [66], if we think of the matrix elements as functions of a parameter α , we cannot, in general, force a crossing by varying α but we must instead take the matrix elements as functions of at least two parameters, which are independently varied. In the one-parameter case one will find that, if two levels approach each other as α is varied, then instead of crossing they will turn away as if repelled.

There is a principal difficulty with the derivation of (3.35). Why should we assume a linear repulsion? Although there are some plausibility arguments for

this form, the result cannot be correct for every system. Furthermore, only the probability arguments cannot explain the nature of a level repulsion. However the situation changes if we intend that statistical properties of the sequence of levels of a real physical system are equivalent to the sequences of eigenvalues of the ensemble of random matrices of a definite symmetry. The theory, based on this hypothesis, was completed in the sixties [67]. The final result for the FNNSDL is

$$P(S) \approx S^\alpha \exp(-\beta S^2). \quad (3.36)$$

The critical index α determining the behaviour of the distribution function at $S \rightarrow 0$ depends on the symmetry of the ensemble of matrices. This symmetry is determined by the properties of the system, the spectrum statistics of which we want to reproduce. If the system is invariant relative to a time reversion, then the corresponding ensemble is a Gaussian orthogonal ensemble (GOA). For the system assuming the violation of the invariance relative to a time reversion, the Gaussian unitary ensemble is associated. Finally, the symplectic ensemble of random matrices corresponds to the Hamiltonian of more complicated structure $H = H_0 + \mathbf{h}\boldsymbol{\tau}$, where $H_0^* = H_0^T$, $h_K = h_K^* = -h_K^T$ ($k = 1, 2, 3$, σ_k — Pauli matrices). The critical index α in formula (3.36) is equal to: $\alpha = 1$ for the GOA, $\alpha = 2$ for the unitary ensembles and $\alpha = 4$ for the symplectic ensembles.

The predictions of the statistical theory of levels (especially for the GOA) were compared in detail with all available sets of nuclear data [65, 67]. No essential deviations between the theory and data base have been revealed. Similar comparisons have been realized for atomic spectra. And here, a good agreement has been revealed with the predictions of the GOA, though the number of processed data was essentially less than in the nuclear spectroscopy.

If for the complicated systems (atomic nucleus, many-electron atom) we can give serious arguments in favour of the hypothesis of the equivalence of the statistical properties of the spectrum and the sequence eigenvalues of the ensemble of the random matrices, so its generalization does not seem natural in the case of the systems with a small number of degrees of freedom.

A radically new and universal approach to the problem of the statistical properties of energy spectra may be developed on the basis of a nonlinear theory of dynamic systems. The numerical calculations [25, 68–71], supported by considerations [1, 3, 7, 25, 52–55, 72–74], show that the important universal peculiarity of the energy spectra of the systems, that are chaotic in the classical limit, is the phenomenon of the level repulsion; while the systems, which dynamics is regular in the classical limit, are characterized by the level clusterization. This statement is sometimes called [68] as the hypothesis of the universal character of the fluctuations of energy spectra.

Among the systems, which spectra were subjected to detailed numerical analysis, the central place is occupied by two-dimensional billiards (free particle

moving on the plane inside of some region and subjecting to the elastic reflection on the boundary). One of two extremal situations can be realized for the billiards with the definite shape of the boundaries: integrable or nonintegrable. The angular momentum is the second integral (except energy) in the circular billiard and such a system is integrable. The billiard like «stadium» is one of the simplest stochastic systems.

The FNNSDL for the integrable system (the circular billiard) is well approximated by Poisson distribution and the variance is the linear function of the considered energy interval, that is in complete correspondence with the hypothesis of the universal character of the fluctuations of energy spectra. In the nonintegrable case («stadium»), the effect repulsion of levels and the slow growth of the variance, caused by the rigidity of the corresponding spectrum, are observed.

Measure of the rigidity is the statistic Δ_3 of Dyson and Mehta [75]

$$\Delta_3(L; x) = \frac{1}{L} \text{Min}_{A,B} \int_x^{x+L} [n(\varepsilon) - A\varepsilon - B]^2 dx \quad (3.37)$$

which determines the least-square deviation of the staircase representing the cumulative density $n(\varepsilon)$ from the best straight line fitting it in any interval $[x, x + L]$. The most perfectly rigid spectrum is the picket fence with all spacing equal (for instance, the one-dimensional harmonic oscillator spectrum), therefore maximally correlated, for which $\Delta_3(L) = 1/12$, whereas, at the opposite, the Poisson spectrum has a very large average value of Δ_3 ($\bar{\Delta}_3 = L/15$), reflecting strong fluctuations around the mean level density.

In contrast to billiards, where the character of motion does not depend on the energy, the Hamiltonian systems are the systems with the separable phase space, which contains both the regions, where the motion is stochastic, along with the islands of stability. How is this circumstance reflected in statistical properties of the spectrum? Berry and Robnik [73] and independently Bogomolny [76], basing on the semiclassical arguments, showed that FNNSDL for such system represents the independent superposition of the Poisson distribution with the relative weight μ , determined by the part of the phase space with regular motion, and the Wigner distribution with the relative weight $\bar{\mu}$ ($\mu + \bar{\mu} = 1$), determined by the part of the phase space with a chaotic motion

$$P(x) = \mu^2 \exp(-\mu x) \text{erfc} \left(\frac{\sqrt{\pi}}{2} \bar{\mu} x \right) + \left(2\mu\bar{\mu} + \frac{\pi}{2} \bar{\mu}^3 x \right) \exp \left(-\mu x - \frac{\pi}{4} \bar{\mu}^2 x^2 \right). \quad (3.38)$$

The expression (3.38) represents the interpolated formula between the Poisson (3.34) and Wigner (3.35) distributions.

Now let us go to the statistical properties of the spectrum of the Hamiltonian of the quadrupole oscillations (3.1). We intend to study the evolution of these properties in the process of R-C-R transition, i. e., in each of energetic intervals R_1, C, R_2 . We shall restrict our consideration to the case of one-well potentials ($W < 16$). At the fixed topology of the potential surface ($W = \text{const}$) the unique free parameter of Hamiltonian (3.1) is the scaled Planck's constant $\bar{\hbar}_i$. In the study of the concrete energetic interval (R_1, C or R_2), corresponding to a definite type of classical motion, the choice of $\bar{\hbar}_i$ is dictated by the possibility of attainment of the necessary statistical assurance (the required number of levels in investigated interval) with conservation of precision of the spectrum calculation (restrictions to possibility of diagonalization of matrices of large dimension). Let us notice, that for the initial nonreduced Hamiltonian (2.3) the variation of $\bar{\hbar}_i$ is equivalent to the variation of the parameters a, b, c (i. e., variation of the critical energies $E_{\text{cr}1}$ and $E_{\text{cr}2}$) or to the adequate choice of the initial Planck's constant $\bar{\hbar}_i \equiv \bar{\hbar}$. The values of the scaled Planck's constant $\bar{\hbar}_3 \equiv \bar{\hbar}$, represented in Table 4, allow us to obtain in the corresponding energy intervals some hundreds of levels with the precision better than 1 %.

Table 4. Scaled Planck's constant $\bar{\hbar}$ for R_1, C, R_2 scaled energy intervals $\Delta\bar{E}$ ($W = 13$)

	R_1	C	R_2
$\Delta\bar{E}$	$\bar{E} < 8 \cdot 10^{-5}$	$8 \cdot 10^{-5} < \bar{E} < 8.4 \cdot 10^{-2}$	$\bar{E} < 8.4 \cdot 10^{-2}$
$\bar{\hbar}$	$\bar{\hbar} = 3.2 \cdot 10^{-6} Z$	$\bar{\hbar} = 1.6 \cdot 10^{-4}$	$\bar{\hbar} = 1.1 \cdot 10^{-1}$

Two additional comments are necessary before proceeding to results. First, we recall that, to get rid of spurious effects of the local properties due to the variation of the density, one has to work at a constant density on the average. For this purpose one can «unfold» the original spectrum [65], i. e., map the spectrum of eigenvalues $\{E_i\}$ onto the spectrum $\{\varepsilon_i\}$ through

$$\varepsilon_i = \bar{N}(E_i). \quad (3.39)$$

Here the smoothed cumulative density $\bar{N}(E)$,

$$\bar{N}(E) = \int_0^E \bar{\rho}(E') dE' \quad (3.40)$$

and $\bar{\rho}(E)$ is the smoothed level density. In what follows we will take as an energy unit the average spacing \bar{x} between two adjacent levels of the unfolded spectrum

$$\bar{x} = \bar{s}_i = \langle (\varepsilon_{i+1} - \varepsilon_i) \rangle. \quad (3.41)$$

Meaning of unfolding is understood by the following example [77]. There are a few spacings between states of the same (J^π, T) in the ground state region known for many nuclei. Together they constitute a large sample of experimental data. The only trouble is that the underlying scaling parameter D varies from nucleus to nucleus. As a result, we cannot make statistical studies unless we have a model for the variation of D as a function of nucleon number A .

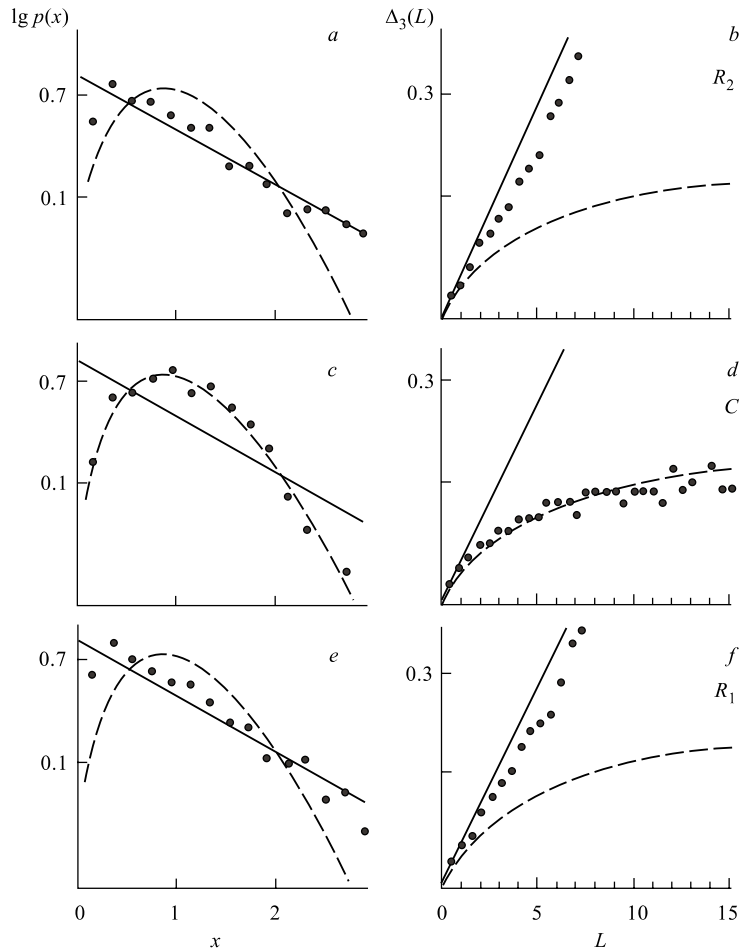


Fig. 14. Fluctuation properties of QON spectrum for the R-C-R transition. Logarithm of $p(x)$ (a, c, e) and average value of Δ_3 (b, d, f); rigid lines are Poisson's prediction; dashed lines are GOA prediction

Second, it should be remarked that our discussion above relative to Poisson of Wigner level statistics applies only for a pure sequence. A pure sequence represents a set of levels relating to one and the same nonreducible representation of the group of symmetry of considered Hamiltonian. In the case of mixed sequences [65] the level repulsion is moderated by the vanishing of Hamiltonian matrix elements connecting two different symmetry states, the spectra have moved towards random, and FNNSDL towards Poisson.

The results of investigation of correlations between statistical properties of energy spectrum of the Hamiltonian QON and the character of classical motion are represented in Fig. 14 [78]. Both the FNNSDL $p(x)$ and the average value of Δ_3 well correspond to the predictions of GOE for the chaotic (C) region. The logarithmic scale for FNNSDL $p(x)$ is suitable to trace this correspondence at large x . For regular regions (R_1 and R_2) the distribution function, in the same scale, according to the hypothesis of the universal character of fluctuations of energy spectra, must be represented by the straight line (the logarithm of Poisson's distribution). The results demonstrate the agreement with this hypothesis, though small-sized deviations are observed for small distances between levels. Such a tendency to the rise of some repulsion in regular region, apparently, is connected with a small admixture of chaotic component. At the construction of statistical characteristics, a purity of sequence is provided by using only those levels, which are relative to definite nonreducible representation of $C_{3\nu}$ group (the levels of E -type were used for results represented in Fig. 14; the statistical characteristics of levels of A_1 - and A_2 -types have similar form).

In this connection brings up the natural question about the role of numerical errors and, in particular, about the special expression «the induced nonregularity» [79]. The investigation of statistical properties of a spectrum in the three-levels model of Lipkin–Meshkov–Glick [80, 81] sheds a certain light on this problem.

3.5. R-C-R Transition and the Structure of QON Wave Function. As we have seen in the previous section, the statistical properties of the spectrum of the Hamiltonian QON have been rigidly correlated with the type of classical motion. It is naturally to try to discover the analogous correlations in the structure of wave functions, i. e., to assume, that the form of the wave function for a semiclassical quantum state, associated with classical regular motion in the regions R_1 or R_2 , is different from that one for chaotic region C . Furthermore, it should be pointed out that in analysis of QMCS at the level of energy spectra the principal role was given to statistical characteristics, i. e., the quantum chaos was treated as a property of the group states. The choice of a stationary wave function of the quantum system, which is chaotic in the classical limit, as a basic object of investigation relates the phenomenon of quantum chaos to an individual state.

In contrast to the spectrum, the form of wave functions depends on the basis. In QMCS studying, the three following representations are used more often:

1. The so-called H_0 representation is: the representation of eigenfunctions $\{\varphi_n\}$ of integrable part H_0 of total Hamiltonian $H = H_0 + V$. The main objects of investigation in this case are the coefficients of expansion C_{mn} of stationary functions ψ_m on basis $\{\varphi_n\}$. H_0 representation is natural in the process of numerical calculations, and H diagonalization is realized more often just in this representation.

2. Coordinate representation in which the behaviour of wave functions simply allows visual comparison with the picture of classical trajectories in coordinate space.

3. Representation with the help of Wigner's functions [82] that has a set of properties, common with a classical function of the distribution in phase space.

As early as in 1977, Berry [83] assumed that the form of the wave function ψ for a semiclassical regular quantum state (associated with classical motion on an N -dimensional torus in the $2N$ -dimensional phase space) was significantly different from the form of ψ for an irregular state, associated with a stochastic classical motion on all or part of the $(2N - 1)$ -dimensional energy surface in phase space. For the regular wave functions the average probability density in the configuration space was seen to be determined by the projection of the corresponding quantized invariant torus onto the configuration space, which implies the global order. The local structure is implied by the fact that the wave function is locally a superposition of a finite number of plane waves with the same wave number as determined by the classical momentum. In the opposite case for the chaotic wave functions the averaged (over small intervals of energy and coordinates) square of the eigenfunctions in the semiclassical limit $\hbar \rightarrow 0$ coincides with the projection of the classical microcanonical distribution to the coordinate space. Its local structure is spanned by the superposition of infinitely many plane waves with random phases and equal wave numbers. The random phases might be justified by the classical ergodicity. This assumption immediately predicts locally the Gaussian randomness for the probability of amplitude distribution. Such structure of the wave function is in good agreement with the picture of chaotic phase space: the classical trajectories homogeneously fill isoenergetic surface. By contrast, from the consideration of a regular quantum state as an analog of a classical motion on torus, a conclusion should be done about the singularity (in limit $\hbar \rightarrow 0$) of the wave function near caustics (boundaries of region of classical motion in coordinate space).

Berry's hypothesis was subjected to the most complete test for billiards of different types and, in particular, for billiard stadium type [84]. The amplitude of a typical wave function of integrable circular billiard is negligible in classical prohibited region (conservation of the angular momentum in circular billiard leads to that the arbitrary trajectory is enclosed between an external and certain internal circle, the radius of which is determined by the angular momentum), whereas near the caustics it is maximal. Distribution $|\psi|^2$ for the case stadium (classical

dynamics is stochastic) is strongly distinguished from the integrable case. However, this distribution is not so homogeneous, as we could expect based on the ergodicity of classical motion.

Let us return to the object of our investigation: C_{3v} symmetric Hamiltonian QON [85, 86]. We start out from the topography of level curves of the stationary wave functions and, in particular, of nodal curves on which $\psi_k(x, y) = 0$. One of a nonrigorous criterion of stochasticity [87] states that the system of nodal curves of the regular wave function is a lattice of quasiorthogonal curves or is similar to such a lattice. At the same time, the wave functions of chaotic states do not have such a representation. Figure 15 confirms that the structure of the lattice of nodal curves of separable wave functions undergoes a change in the R-C-R transition. The spatial structure of nodal curves for states from regions R_1 (g, h, i) and R_2

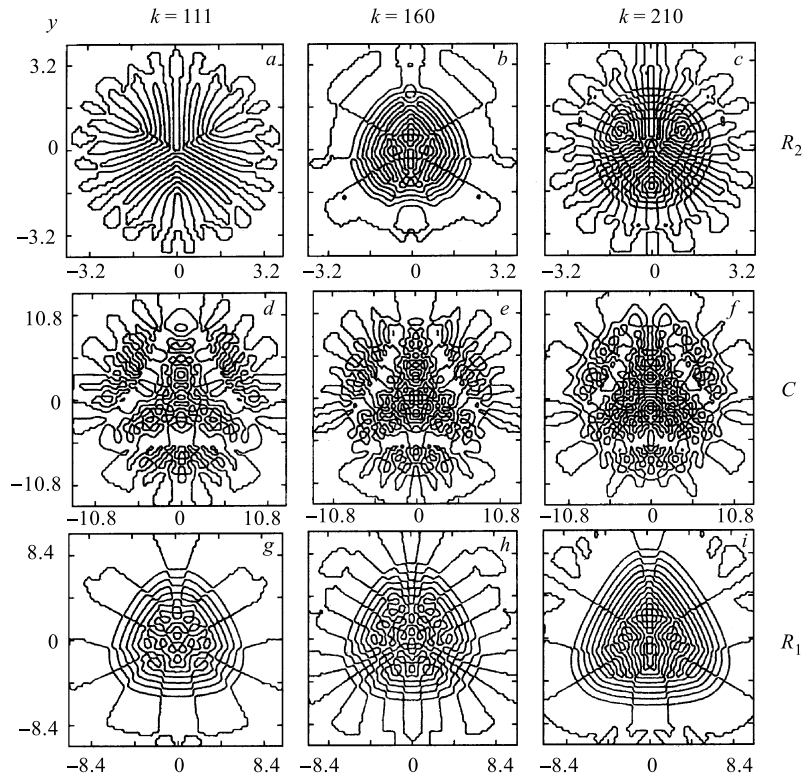


Fig. 15. Nodal curves of the wave functions $\psi(x, y)$. The numbers k of the corresponding levels are shown over the figures: a, d, g) $k = 111$; b, e, h) $k = 160$; c, f, i) $k = 210$

(*a, b, c*) of regular classical motion is considerably simpler than this structure for states from the chaotic region *C* (*d, e, f*).

Correlations between the structure of wave function and the type of classical motion are also demonstrated in Fig. 16, in which the probability density

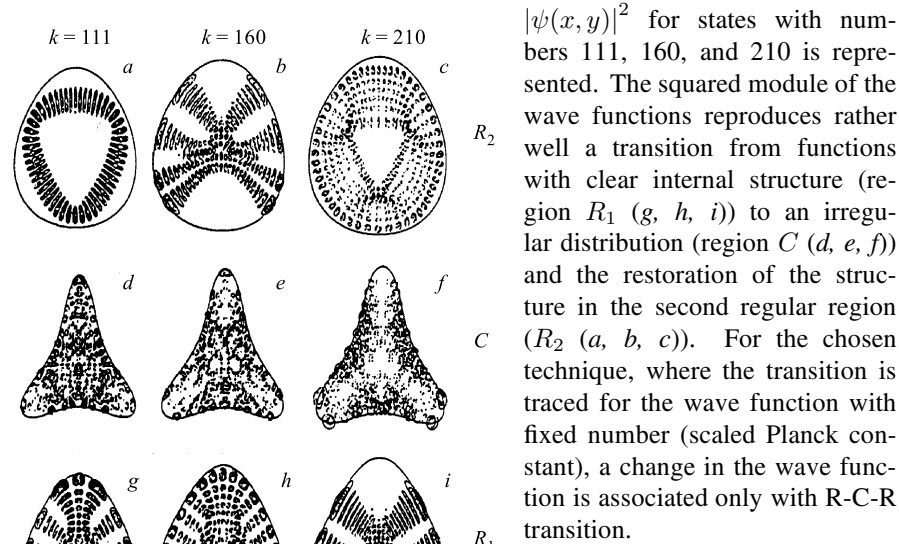


Fig. 16. Isolines of the probability density $|\psi_k(x, y)|^2$. The numbers k of the corresponding levels are shown over the figures: *a, d, g*) $k = 111$; *b, e, h*) $k = 160$; *c, f, i*) $k = 210$

$|\psi(x, y)|^2$ for states with numbers 111, 160, and 210 is represented. The squared module of the wave functions reproduces rather well a transition from functions with clear internal structure (region R_1 (*g, h, i*)) to an irregular distribution (region *C* (*d, e, f*)) and the restoration of the structure in the second regular region (R_2 (*a, b, c*)). For the chosen technique, where the transition is traced for the wave function with fixed number (scaled Planck constant), a change in the wave function is associated only with R-C-R transition.

Evolution of the wave functions in the process of R-C-R transition can be studied also in H_0 -representation or more appropriately in the representation of linear combinations of wave functions of two-dimensional harmonic oscillator with equal frequencies (see Sec. 3.2)

$$\psi_k = \sum_{N,L} C_{NLj}^k |NLj\rangle. \quad (3.42)$$

The introducing of the notion of distributivity of the wave function on basis leads to the criterion of stochasticity formulated by Nordholm and Rise [88]. It states that the degree of distributivity of wave functions arises in the average along with the degree of stochasticization. It is clear that this criterion is a direct analog of the Berry's hypothesis for H_0 -representation, if the number of basis state $i\{NLj\}$ is to be interpreted as a discrete coordinate. Figure 17 qualitatively confirms this criterion. It can be seen from this figure that the states corresponding to regular motion are distributed in a relatively small number of basis states. At the same

time, the states corresponding to chaotic motion (region C) are distributed in a considerably larger number of basis states. In the latter case, the contributions from a large number of basis states in expansion (3.42) interfere. This reflects in a complex spatial structure of the wave function $\psi_k(x, y)$.

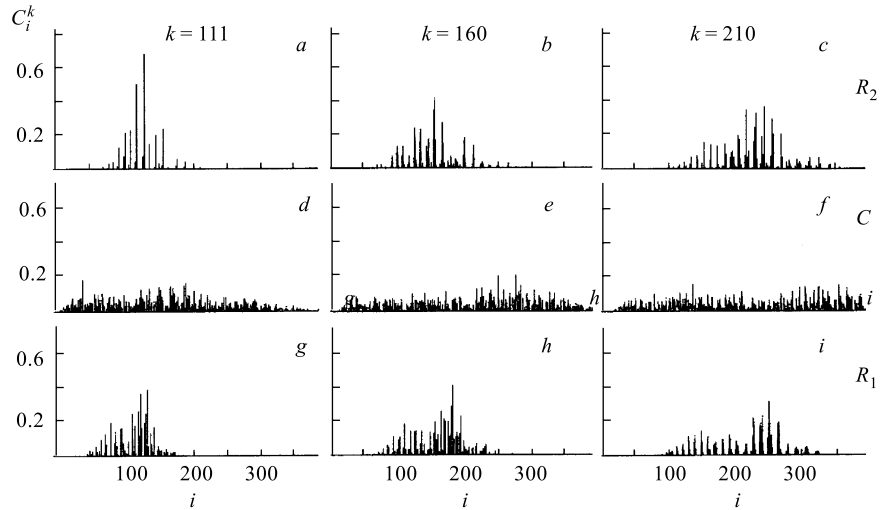


Fig. 17. Distribution of the coefficient C_i^k in the number $i = (N, L, j)$ of the basis state. The numbers k of the corresponding levels are shown over the figures: a, d, g) $k = 111$; b, e, h) $k = 160$; c, f, i) $k = 210$

3.6. Evolution of Shell Structure in the Process of R-C-R Transition.

Introduction of the stochasticity concept in the nuclear theory made possible taking a fresh look [16] at the old paradox [24]: how one could reconcile the liquid drop — short mean free path-model of the nucleus with the independent particles — gas-like shell model. To solve this paradox within the limits of philosophy of simple chaos (see Sec. 1.1) it is sufficient to assume [18]:

1) When the nucleonic motion inside the nucleus is integrable, one expects to see strong shell effects in nuclear structure, quite well reproducible, for example, by the model of independent particles in the potential well.

2) If a chaotic component dominates in the nuclear dynamics, it is necessary to expect that the droplet model or Thomas–Fermi approximation will appear more useful.

At such approach, the elucidation of the mechanism of destruction of shell effects in the process of the R-C transition plays the key role. More appropriately the problem can be formulated in the following way [16]: how do shell dissolve with deviations from integrability or, conversely, how do incipient shell effects emerge as the system first begins to feel its proximity to an integrable situation?

As has been mentioned above, the finite motion of the integrable Hamiltonian system with N degrees of freedom is, in general, conditionally periodic, and the phase trajectories lie on N -dimensional tori. In the variables action-angle (I, θ) the Hamiltonian is cyclic with respect to angle variables, $H = H_0(I)$. Poincare called the main problem of dynamics the problem about the perturbation of conditionally periodic motion in the system defined by the Hamiltonian

$$H = H_0(I) + \varepsilon V(I, \theta), \quad (3.43)$$

where ε is a small parameter. The essential step in the solution of this problem was the KAM theorem, asserting that at switching on nonintegrable perturbation, the majority of nonresonance tori, i. e., the tori for which

$$\sum_{i=1}^N n_i \frac{\partial H_0}{\partial I_i} \neq 0, \quad (3.44)$$

is conserved, distinguishing from the nonperturbed cases only by a small (to the extent of smallness of ε) deformation. As is known, at definite conditions the KAM formalism allows one to remove the members depending on angle out of Hamiltonian, using the convergent sequence of canonical transformations [4]. When it is succeeded, we find that perturbed motion lies on rather deformed tori so that trajectories, generated by perturbed Hamiltonian, remain quasiperiodic. In other words, the KAM theorem reflects an important peculiarity of classical integrable systems to conserve regular behaviour even at rather strong nonintegrable perturbation. In the problem of our interest, concerning the destruction of a shell structure of the quantum spectrum, the KAM theorem also will be able to play an important role. Considering the residual nucleon–nucleon interaction as nonintegrable addition to selfconsistent field, obtained, for example, in Hartree–Fock approximation [33], one can try to connect the destruction of shell with the deviation from integrability. The existence of shell structure at rather strong residual interaction (or at large deformation) can be obligated to rigidity of KAM tori, contributing to survival of regular behaviour. Such assumption seems rather natural, especially if one takes into account, that the procedure of quasiclassical quantization [89, 90] itself as well as KAM theorem is based on convergence of the same sequence of canonical transformations.

The aim of this section is to trace the evolution of the structure of QON Hamiltonian. In numerical calculations of this section it will be more convenient to use nonscale version of the Hamiltonian (2.3). By nonperturbed Hamiltonian H_0 we will mean the Hamiltonian of two-dimensional harmonic oscillator with equal frequencies: $H_0 \equiv H(a = 1, b = 0, c = 0)$. Its degenerate equidistant spectrum is well known. At switching on perturbation, the degeneration disappears and the shell structure forms. The number of states, for example, the states of

E -type (the numerical results, represented below, are relative to the states of this type, while analogous results take place for the states belonging to another nonreducible representations of $C_{3\nu}$ -group) for the given quantum number N is equal to $1/2(N_1 + \text{Mod}(N, 2))$, where $N_1 = 1/3(2N + \text{Mod}(N, 3))$, and $\text{Mod}(N, M)$ is a remainder from division of N by M .

It is obvious, that eigenfunctions of exact Hamiltonian QON are no longer the eigenfunctions of operators \hat{N} and \hat{L} . Nevertheless, as numerical calculations show, one can use the quantum numbers N and L for the classification of wave functions even at rather large nonlinearity. The measure of nonlinearity, at which such classification (i. e., the existence of shell structure) remains reasonable, is connected with quasicrossing of neighbouring levels. Under the quasicrossing we shall understand the approach of levels up to the distances of degree of precision of numerical calculations.

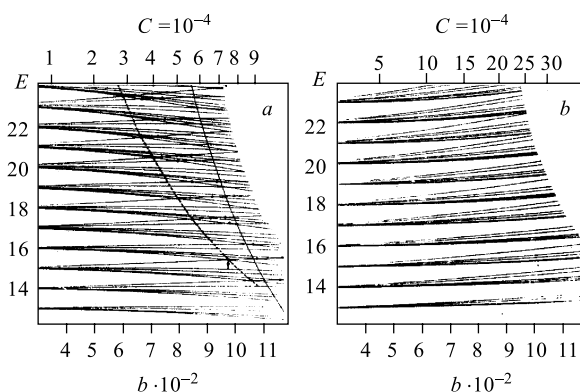


Fig. 18. *a*) Energy spectra of Hamiltonian (2.3) depending on parameter b ($W = 13$). Points mark quasicrossings. Continuous line-dependence E_{cr} from b . Dashed line shows the beginning of the region of quasicrossings. The arrow shows the point of quasicrossing of the levels with $k = 40$ and 41 . *b*) The same for $W = 3.9$

The dependence of the energy spectra of Hamiltonian QON on the parameter b for the values $W = 3.9$ and 13 are represented in Fig. 18, *a*, *b*. As is seen from Fig. 18, *a*, for the PES with $W = 13$ at the approaching to the line of the critical energy of the transition to chaos, defined according to the NCC, the destruction of shell structure, by which we understand multiple beginning of quasicrossing, takes place. At the same time, for the PES with $W = 3.9$ in Fig. 18, *b* (for which as we have shown in Sec. 2.2, the local instability is absent and the motion is regular at all energies) the quasicrossings are absent even at larger nonlinearity than for $W = 13$.

The destruction of shell structure can be traced for the wave functions, using the analog of thermodynamic entropy S_k [91, 92],

$$S^k = - \sum |C_{NLj}^k|^2 \ln |C_{NLj}^k|^2. \quad (3.45)$$

The character of changes of entropy in regions R_1 and R_2 , corresponding to the regular classical motion, correlates with the transition from shell to shell (see

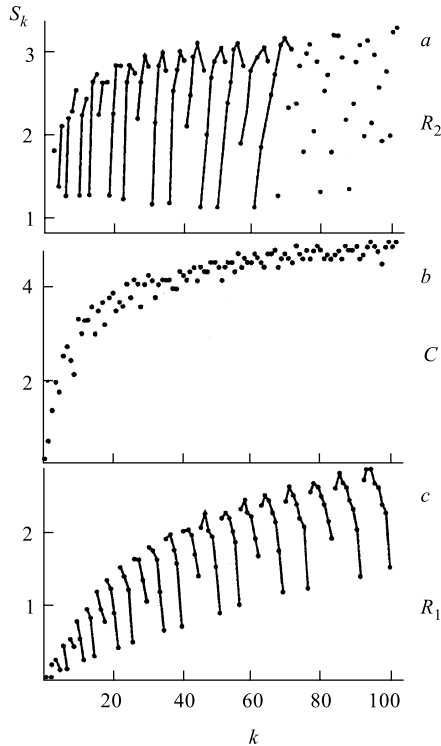


Fig. 19. Entropy S as a function of state number k

sification of levels with the help of quantum numbers N and L loses its sense.

Notice, that we could observe restoration of shell structure at high energies in the process of R-C transition only due to the optimization of basis frequency (see Sec. 3.2), that is equivalent to the possibility of diagonalization of matrices of considerably higher dimension.

Fig. 19, *c, a*). Two effects are observed in the region C (Fig. 19, *b*), corresponding to chaotic classical motion. Firstly, quasiperiodical dependence of entropy from energy is violated, that testifies to destruction of shell structure. Secondly, the monotone growth of entropy is observed on average with going out on plateau corresponding to the entropy of random sequence at the energies essentially exceeding the critical energy.

Average values of operator \hat{N} , given in Fig. 20, and calculated on stationary wave functions of an exact Hamiltonian, describe the dynamics of change of the shell structure. We can see that the minimum deviation of $\langle N \rangle$ from N is observed in regions R_1 (*c*) and R_2 (*a*), while this deviation is considerably greater in the stochastic region C (*b*); moreover in the average it monotonically increases with the increase of energy. It is obvious, that at energies, for which $N - \langle N \rangle \geq 1$, the destruction of quantum analogues of classical integrals leads to the fact that the clas-

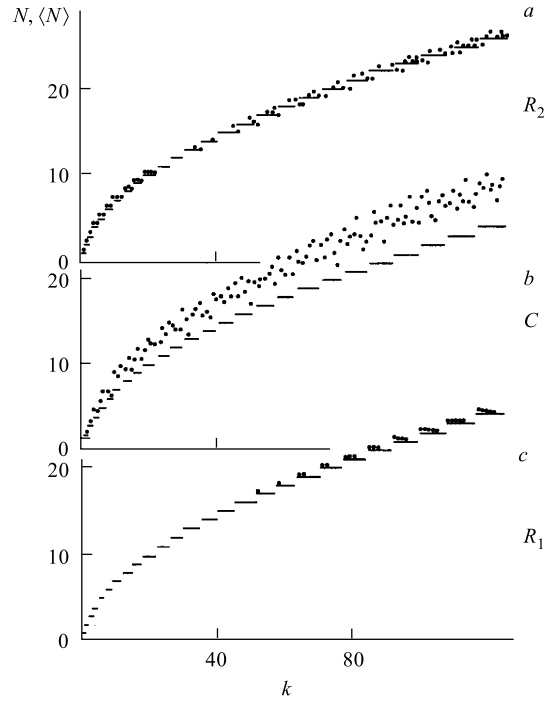


Fig. 20. N (lines) and $\langle N \rangle$ (points) as a function of the number k

Now let us return to the analysis of quasicrossings of levels arising near the critical energy of the transition to chaos. As is known [93], for the set of Hamiltonians depending on two parameters $\lambda = (b, c)$, which are invariant with respect to inversion of time in the neighbourhood of the degeneration point $\lambda^* = (b^*, c^*)$, the difference of two terms $\Delta E = E_1 - E_2$ is determined by the expression

$$\Delta E(b, c) = [A(b - b^*)^2 + B(b - b^*)(c - c^*) + C(c - c^*)^2]^{1/2}, \quad (3.46)$$

where coefficients A, B, C are the functions of components $\nabla_\lambda H$ in the point λ^* . The characteristics of nuclear shape [94] in the problems of nuclear spectroscopy more often play the role of parameters. The wave functions of intersecting levels near a degeneration point can be represented in the following form

$$\begin{aligned} |E_1(\lambda)\rangle &= \cos \chi_1 |E_1(\lambda^*)\rangle + \sin \chi_1 |E_2(\lambda^*)\rangle, \\ |E_2(\lambda)\rangle &= \cos \chi_2 |E_1(\lambda^*)\rangle + \sin \chi_2 |E_2(\lambda^*)\rangle, \end{aligned} \quad (3.47)$$

where angles of mixing $\chi_{1,2}$ are determined by the relation

$$e^{2i\chi_{1,2}} = \pm \frac{(T\lambda) + i(S\lambda)}{[(T\lambda)^2 + (S\lambda)^2]^{1/2}}, \quad (3.48)$$

$$(T\lambda) \approx H_{11}(\lambda) - H_{22}(\lambda), \quad (S\lambda) \approx 2H_{21}(\lambda).$$

It is easy to see, that changing $\lambda \rightarrow -\lambda$, the «exchange» of wave functions of approaching levels takes place $|E_1(\lambda^*)\rangle \leftrightarrow |E_2(\lambda^*)\rangle$. Such test can be used effectively for the analysis of nature of quasicrossing points.

In particular, we trace the variations of functions with $k = 40$ and $k = 41$, which undergo quasicrossing in the neighbourhood $b^* \approx 9.8 \cdot 10^{-2}$, $c^* \approx 7.4 \cdot 10^{-4}$ (recall, that under this term we understand the approaching of levels up to distances of an order of precision of numerical calculations). The sections of $\psi(x=0, y)$ and coefficients of expansions C_{NLj}^k of wave functions of considered states before and after a quasicrossing point are represented in Figs. 21, 22. For comparison, the similar characteristics of the states with $k = 39$ and $k = 42$ which do not undergo quasicrossing at this values of parameters are represented for comparison at the same figure. As is seen, the wave functions are not

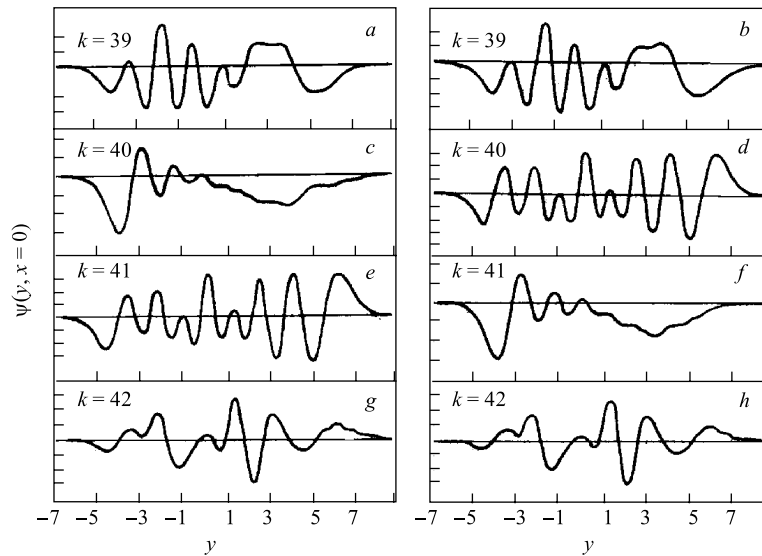


Fig. 21. Wave functions $\psi(x=0, y)$ for the states with $k = 39$ (a, b), 40 (c, d), 41 (e, f), 42 (g, h) in the neighbourhood of quasicrossing of the states with $k = 40$ and 41: a, c, e, g) $b < b^*$; b, d, f, h) $b > b^*$ (point of quasicrossing: $b^* = 0.098$, $c^* = 0.00074$)

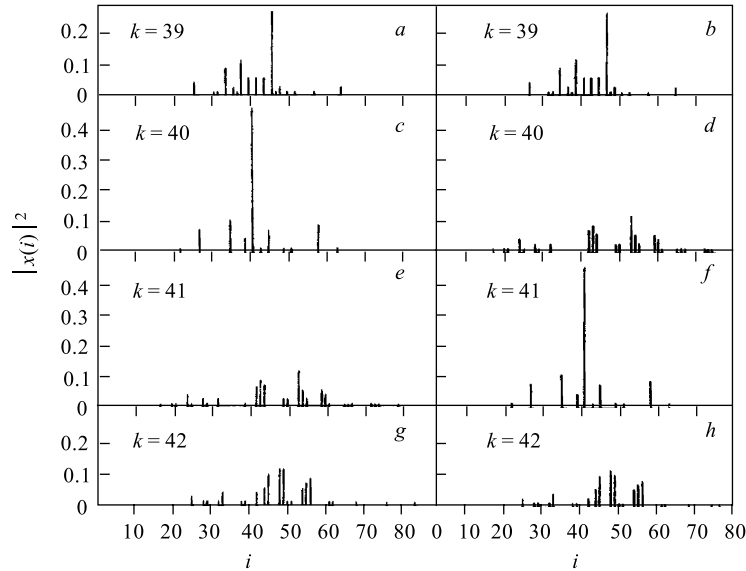


Fig. 22. Same as Fig. 21, but for the coefficients of the expansion of wave functions $|x(i)|^2 = |C_{NLj}^{(k)}|^2$, i — number of basis state

practically changed for the states 39 and 42, at the same time the exchange of wave functions is observed for the states 40 and 41 in correspondence with the test described above. An analogous situation takes place for other quasicrossings as well.

3.7. Wave Packet Dynamics. The investigation of the time evolution of non-stationary states, i. e., of packets in quantum systems which classical analogues admit chaotic behaviour, gives an important information about QMCS. The localized quantum wave packet (QWP) is the closest analogue of the point in phase space, which describes the state of a classical system. However, such correspondence between localized QWP and a classical point particle in the chaotic region is broken down for a very short time interval. Let us explain this fact by using Takahashi arguments [95]. We take two localized QWP $\Psi_1(\mathbf{x})$ and $\Psi_2(\mathbf{x})$ which are put in the chaotic region at initial time to be slightly different from each other so that the difference between $\langle \Psi_1 | \hat{\mathbf{x}} | \Psi_1 \rangle$ and $\langle \Psi_2 | \hat{\mathbf{x}} | \Psi_2 \rangle$ (or $\langle \Psi_1 | \hat{\mathbf{p}} | \Psi_1 \rangle$ and $\langle \Psi_2 | \hat{\mathbf{p}} | \Psi_2 \rangle$) is very small. We assume that in the chaotic region the localized QWP does not either extend in a certain time interval of the order $1/\sqrt{\hbar}$ like that in the regular region. Thence, following the Ehrenfest theorem, the packets Ψ_1 and Ψ_2 move as classical particles and the distance between $\langle \Psi_1 | \hat{\mathbf{x}} | \Psi_1 \rangle$ and $\langle \Psi_2 | \hat{\mathbf{x}} | \Psi_2 \rangle$ (or $\langle \Psi_1 | \hat{\mathbf{p}} | \Psi_1 \rangle$ and $\langle \Psi_2 | \hat{\mathbf{p}} | \Psi_2 \rangle$) is increasing exponentially in time.

Let us consider the superposition $\Psi = \Psi_1 + \Psi_2$, which also becomes a localized QWP in initial state. From the assumption, we can expect that QWP does not extend in a certain time interval of the order $1/\sqrt{\hbar}$. However, considering the exponential increment of the distance between $\langle \Psi_1 | \hat{x} | \Psi_1 \rangle$ and $\langle \Psi_2 | \hat{x} | \Psi_2 \rangle$, Ψ extends exponentially in the chaotic region and does not behave as a classical particle. This result is inconsistent with the initial assumption and implies that in the chaotic region the localized QWPs (i. e., $\Psi_1(\mathbf{x})$, $\Psi_2(\mathbf{x})$, and $\Psi(\mathbf{x})$) extend exponentially as does classical probability distribution in the first stage of time development.

In order to describe such unusual behaviour of QWP one should address to the concept of a quantum-mechanical phase space. There are a few well-established schemes to introduce phase-space variables in quantum mechanics [82, 96, 97]. In the present study we shall follow the procedure proposed by Weissman and Jortner [98]. Let us consider an initially localized QWP Ψ characterized by the coordinates \mathbf{q} and the momenta \mathbf{p} ,

$$\mathbf{q} = \langle \Psi | \hat{\mathbf{q}} | \Psi \rangle, \quad \mathbf{p} = \langle \Psi | \hat{\mathbf{p}} | \Psi \rangle. \quad (3.49)$$

Now we introduce the coherent states $|\mathbf{p}, \mathbf{q}\rangle$ [97], which in the coordinate x representation, are given by Gaussian wave packets

$$\langle \mathbf{x} | \mathbf{p}, \mathbf{q} \rangle = \prod_{j=1}^N (\pi \sigma_j^2)^{-1/4} \exp \left[-\frac{(x_j - q_j)^2}{2\sigma_j^2} + \frac{i p_j x_j}{\hbar} - \frac{i p_j q_j}{2\hbar} \right]. \quad (3.50)$$

In the study of a system of N coupled harmonic oscillators, it is convenient to choose for constants σ_j the rms zero-point displacements

$$\sigma_j = (\hbar/m_j \omega_j)^{1/2}, \quad (3.51)$$

where m_j are masses and ω_j are frequencies of the uncoupled oscillators. With this choice of the σ_j , the coherent states $|\alpha\rangle \equiv |\mathbf{p}, \mathbf{q}\rangle$ become the eigenstates of the harmonic oscillator annihilation operators a_j

$$a_j |\alpha\rangle = \alpha_j |\alpha\rangle, \quad (3.52)$$

where a complex variable α_j

$$\alpha_j = \frac{1}{\sqrt{2}} \left(\frac{q_j}{\sigma_j} + i \frac{\sigma_j}{\hbar} p_j \right). \quad (3.53)$$

Using these coherent states, it is possible to introduce the following quantum-mechanical phase-space density

$$\rho_\Psi(\mathbf{q}, \mathbf{p}) = |\langle \alpha | \Psi \rangle|^2, \quad (3.54)$$

where Ψ is any general wave packet. This quantum-mechanical, coherent-state, phase-space density may be regarded as a quantum analogue of the classical phase-space density, since it satisfies an equation of motion where the leading term (when expanded in powers of \hbar) corresponds to the classical Liouville equation [99]. The stationary phase space densities $\rho_E(\mathbf{p}, \mathbf{q})$ are the

$$\rho_E(\mathbf{p}, \mathbf{q}) = |\langle \alpha | E \rangle|^2, \quad (3.55)$$

where $|\alpha\rangle$ is given in terms of Gaussian wave packets (3.50) while the eigenstate $|E\rangle$ is given by squares of the projections of the eigenstates on the coherent state, Eq. (3.4). Using the well-known expressions for scalar products $\langle \alpha | NL \rangle$ [97] we finally obtain

$$\begin{aligned} \rho_E(\mathbf{p}, \mathbf{q}) = & \frac{1}{2} \exp \left[-\frac{1}{2} \left(|\alpha_+|^2 + |\alpha_-|^2 \right) \right] \times \\ & \times \sum_{N,L} \frac{C_{NL}}{(n_+! n_-!)^{1/2}} \left(\alpha_+^{*n_+} \alpha_-^{*n_-} + j \alpha_+^{*n_-} \alpha_-^{*n_+} \right), \end{aligned} \quad (3.56)$$

where $\alpha_{\pm} = 1/\sqrt{2}(\alpha_2 \mp i\alpha_1)$ with $\alpha_{1,2} = 1/\sqrt{2}(q_{1,2} + ip_{1,2})$, $n_+ = \frac{N+L}{2}$, $n_- = \frac{N-L}{2}$, $j = \pm 1$. The phase-space density $\rho_E(\mathbf{p}, \mathbf{q})$ is a function of the four real variables p_1, q_1 and p_2, q_2 .

We can get the contour maps of $\rho_E(p_1, q_1; p_2, q_2)$ in the (q_2, p_2) plane, taking $q_1 = 0$ and calculating p_1 from the relation

$$H(q_1 = 0, p_1, q_2, p_2) = E. \quad (3.57)$$

Such obtained quantum Poincaré maps (QPM) [98], constitute the quantum analogues of the classical Poincaré maps and can be used for the search of QMCS both in the structure of wave functions of stationary states and in the dynamics of wave packets.

Next, let us consider the time evolution of a wave packet, which is initially in a coherent state

$$|\Psi(t=0)\rangle = |\alpha\rangle. \quad (3.58)$$

The time evolution of such initiality coherent wave packet is given by

$$|\Psi(t)\rangle = \sum_k |E_k\rangle \langle E_k | \alpha \rangle e^{-iE_k t}. \quad (3.59)$$

The survival probability $p(t)$ of finding the system in its initial state is

$$p(t) = |g_{\alpha}(t)|^2, \quad (3.60)$$

where $g_\alpha(t)$ is the overlap of $\Psi(t)$ with the initial state

$$g_\alpha(t) = \langle \alpha | \Psi(t) \rangle = \sum_k |\langle E_k | \alpha \rangle|^2 e^{-iE_k t}. \quad (3.61)$$

Utilizing the definition of the stationary phase-space density (3.55), we can write

$$g_\alpha(t) = \sum_k \rho_{E_k} e^{-iE_k t}. \quad (3.62)$$

Equation (3.62) implies that dynamics is determined by the spectrum of the initial coherent state $|\alpha\rangle$.

Weissman and Jortner [98] have observed for Henon–Heiles Hamiltonian (QON Hamiltonian with $m = 1$, $a = 1$, $c = 0$) two limiting types of QWP dynamics of initially coherent Gaussian wave packets, which correspond to a quasiperiodic time evolution and to rapid decay of the initial state population probability. A quasiperiodic time evolution is exhibited by wave packets initially located in regular region, while a rapid decay of the initial state population probability is revealed by those ones that are initially placed in irregular regions.

Ben-Tal and Moiseyev [100] calculated the survival probability $p(t)$ for the initial complex Gaussian wave packets by the Lanczos recursion method. This method has a practical value since it requires nN^2 numerical operations (n is the number of Lanczos recursion, N is the dimension of the Hamiltonian matrix) rather than N^3 required to calculate the eigenvectors H . For bounded time calculations n is much smaller than N .

Let us turn to the consideration of the dynamics of QWP in the PES with a few local minima ($W > 16$) [101]. Transitions between different local minima can be divided into induced (the excitation energy exceeds the value of the potential barrier) and tunnel transitions. The latter ones are subdivided into transitions from a discrete spectrum into a continuous spectrum (for example, α -decay, spontaneous division) and from a discrete spectrum into a discrete spectrum (for example, transitions between isomeric states). Up to now the process of tunneling across a multidimensional potential barrier, when initial and final states are in a discrete spectrum, is the most complicated and almost noninvestigated problem.

More often the time evolution of a wave packet is studied by two methods [102]: either by direct numerical integration of the Schrödinger time-dependent equation with corresponding initial condition $\Psi(\mathbf{r}, t = 0)$, or by expansion of the packet $\Psi(\mathbf{r}, t)$ in the eigenfunctions of the stationary problem. The first one has some lacks, e. g., the complication relative to interpretation of the obtained results and the necessity of separating the contributions from subbarrier and tunnel transitions for the packet of an arbitrary shape. These difficulties can be avoided by providing the subbarrier part of the spectrum $E_n (E_n < U_0, U_0 - \text{the height of barrier})$ and the corresponding stationary wave functions $\psi_n(\mathbf{r})$ to be known. A

pure tunnel dynamics will take place for the packets representable in the form

$$\Psi(\mathbf{r}, t) = \sum_n C_n \exp\left(-\frac{i}{\hbar} E_n t\right) \psi_n(\mathbf{r}), \quad E_n < U_0, \quad (3.63)$$

$$C_n = \int \Psi(\mathbf{r}, t=0) \psi_n(\mathbf{r}) d\mathbf{r}. \quad (3.64)$$

The probability $p^R(t)$ of finding the particle at the moment of time t in certain local minimum R is

$$p^R(t) = \int_R |\Psi(\mathbf{r}, t)|^2 d\mathbf{r} = \sum_{m,n} C_m^* C_n \exp\left(\frac{i(E_m - E_n)t}{\hbar}\right) \int \psi_m^*(\mathbf{r}) \psi_n(\mathbf{r}) d\mathbf{r} \quad (3.65)$$

or in the two-level approximation

$$p^R(t) = p^R(0) - 4C_1 C_2 \sin^2\left(\frac{1/2(E_1 - E_2)t}{\hbar}\right) \int \psi_1^*(\mathbf{r}) \psi_2(\mathbf{r}) d\mathbf{r}. \quad (3.66)$$

Let us introduce [103] the value

$$\bar{p}^R = \max_{\forall t} p^R(t) \quad (3.67)$$

which is the maximum probability of finding the particle in the certain local minimum R if initially it was localized in the arbitrary minimum. If the number of local minima is more than two, then of independent interest is

$$\bar{p}^{R_0} = \min_{\forall t} p^{R_0}(t), \quad (3.68)$$

i. e., minimum probability to find the wave packet in the minimum R_0 corresponding to its initial localization.

Intuitively, we may suggest that $\bar{p}^R \approx 1$ if the initial minimum is local, and the final one is absolute. However, the results [103] obtained for the simplest one-dimensional models (asymmetric double wells of different shapes) are inconsistent with the intuitive expectations. The probability of tunneling from the local minimum to the absolute one depends resonantly on the potential parameters. Figure 23, *b* gives the dependence of \bar{p}^R on the well depth displacement d . It is seen that at an arbitrary asymmetry $\bar{p}^R \ll 1$.

The resonant behaviour of \bar{p}^R becomes more clear if one considers the spatial structure of the subbarrier wave functions. For a sufficiently wide barrier in the case of an arbitrary asymmetry, the subbarrier wave functions are largely localized in separate minima. The delocalization takes place only in the vicinity of the level quasicrossing. The degree of this delocalization directly depends on the distance

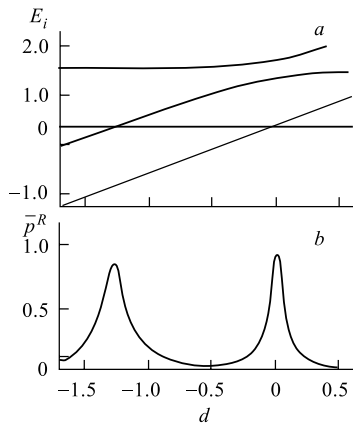


Fig. 23. Subbarrier energy levels E_i for a double asymmetric one-dimensional rectangular well with infinite external walls (a) and \bar{p}^R (b) as a function d . Width of the well is equal to 3; width of barrier, to 1; height of barrier, to 2

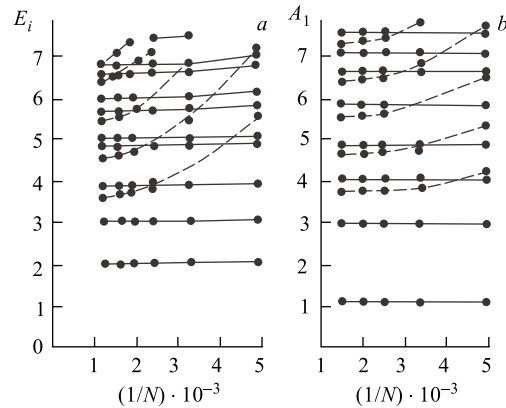


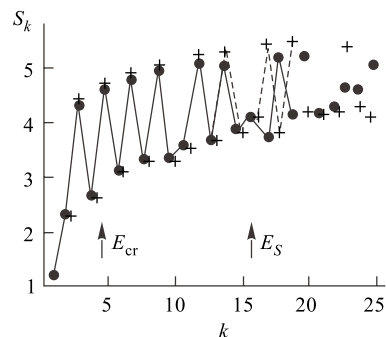
Fig. 24. Dependence of the energy spectrum of E type (a) at $b=0.173798$ and A_1 type (b) at $b=0.17$ from the dimension of submatrices N for $W=17.8$

between the interacting levels. Obviously, the QWP, in which the components localized in the certain minimum are dominating, cannot tunnel effectively to the neighbouring minimum. It is precisely this, that explains the stringent correlation between the \bar{p}^R minima and the level quasicrossing (see Fig. 23).

Now the question arises if a similar correlation between the level quasicrossings, the delocalization of wave functions and the resonant tunneling persists in the two-dimensional case. To give an answer to this question let us turn to Hamiltonian QON in the region $W > 16$. Recall that three ($C_{3\nu}$ -symmetry) identical additional minima appear at $W > 16$ apart from the central minimum. The central minimum exceeds the lateral ones in depth in the region $16 < W < 18$. At $W > 18$, the central minimum becomes the local one. In this region of parameters, the procedure of diagonalization of Hamiltonian QON in an oscillator basis becomes essentially complicated. It is connected with the fact, that the basis of Hamiltonian, the potential of which has the unique minimum, is used for the diagonalization of Hamiltonian possessing complex topology of the PES. In addition to the large dimension of the basis it is necessary for the basis wave functions to have a sufficient value in the region of the lateral minima. It has been achieved by the optimization of oscillator frequency of basis ω_0 . For the values of parameters used in the calculations ($W = 17.8, b = 0.17$) the value of oscillator frequency $\omega_0 = 0.2$. Figure 24 gives low eigenvalues of E and A_1 types depending on the basis dimension. We can see, that it is possible to get

the saturation in the basis at the dimension of submatrices $N \sim 10^3$ even for low states localized in the lateral minima (dashed lines).

Fig. 25. Dependence of S_k from a number of eigenstate k (A_1 type) for the dimension of submatrices 408 (dark point) and 690 (crosses) at $W = 17.8$ and $b = 0.17$; E_S corresponds to saddle energy; and E_{cr} , the classical critical energy of the transition from regular type of motion to chaotic one



We can also use the above-introduced analog of thermodynamic entropy S_k for estimation of degree of saturation in the basis. Figure 25 gives the S_k values for the states of A_1 type for the dimension of submatrices 408 and 690. Increasing of the basis does not lead to sufficient changes of values S_k for the states with the energy up to the saddle energy E_S .

The states, localized in the central or in the lateral minima, have an essentially different distributivity of coefficients $C_i^k C_i^k \{i \equiv NLj\}$ (see Fig. 26, *a*, *b*) and thus different entropies: states, localized in the central minimum, have less entropy). In the neighbourhood of the points of level quasicrossings, the delocalization of wave functions, corresponding to these levels, takes place; these wave functions possess close distributivity of coefficients C_i^k (see Fig. 26, *c*, *d*).

Figure 27 shows the subbarrier part of the energy spectrum obtained by the diagonalization. As is easy to see, the tunneling of the wave packet, composed

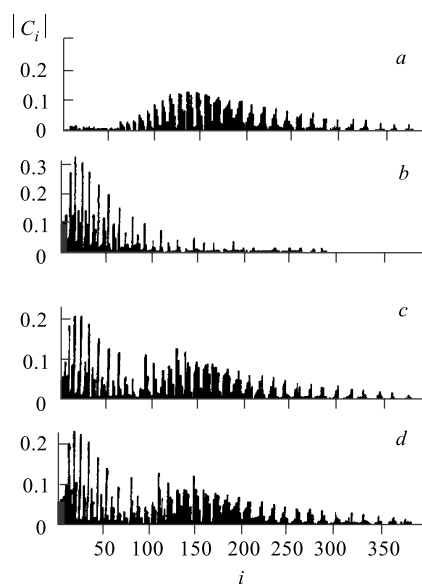


Fig. 26. Distribution of coefficients $|C_i|$ by number of basis state $i = (NLj)$ (E type) for the localized states with $k = 3$ (*a*) and $k = 4$ (*b*) at $b = 0.17379$ ($W = 17.8$) and for the delocalized states with $k = 3$ (*c*) and $k = 4$ (*d*) in the point of quasicrossing $b = 0.1737924$ ($W = 17.8$)

of the subbarrier wave functions, can be described in the two-level approximation. Indeed, there are approximately 10 level quasicrossings of A_1 and E types,

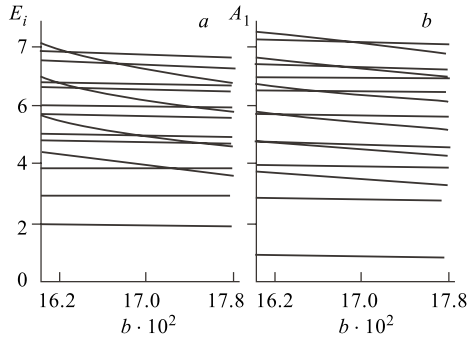


Fig. 27. Dependence of energy levels E_i of Hamiltonian (2.3) on the parameter b for $W = 17.8$: a) spectrum of E type; b) spectrum of A_1 type

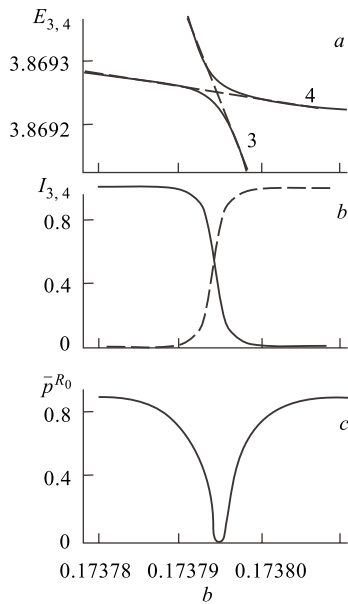


Fig. 28. a) Quasicrossing of energy levels of E type with $K = 3, 4$ for Hamiltonian (2.3); b) localization of wave functions of states with $k = 3, 4$ in the central well at different b ; c) dependence \bar{p}^{R_0} from b

where the nonlinearity parameter changes are of the order of 10^{-2} . The effective half-width of the overlap integral in (3.66) is about 10^{-5} (see Fig. 28). Hence, all nondiagonal elements will be close to zero with the overwhelming probability in the matrix $\alpha_{mn} = \int_R \psi_m^*(\mathbf{r})\psi_n(\mathbf{r})d\mathbf{r}$ for an arbitrary nonlinearity parameter (e. g., b). Two appreciable different from zero nondiagonal matrix elements (two-level approximation) appear only in the vicinity of quasicrossings. The probability of double quasicrossings at a fixed nonlinearity parameter is almost excluded. This probability is by two or three orders lower than that of rather rare ($\sim 10^{-3}$) single quasicrossings.

So, now we can give the answer to the question we have posed above. The most stringy correlations between level quasicrossings, delocalization of wave functions and resonant tunneling across the potential barrier take place in the two-dimensional case (and, most likely, in the multidimensional one, too).

The existence of the mixed state for the many-well potentials must be well self manifested in dynamics of the QWP. Preexponential

factor of the tunnel amplitude depends on the type of classical motion and consequently we expect to observe the asymmetry of the effective barrier penetration in the mixed. This purely classical effect may be observed only if the uncertainty in the level energy is comparable with the average distance between levels and the system does not yet «feels» that the spectrum is discrete. This determines the time scale for which the observation of the effect is possible. It is the same time scale on which the transition from the classical linear diffusive increasing of the energy to quasiperiodical quantum evolution is observed [104].

3.8. Chaotic Regimes in Reactions with Heavy Ions. Outlined in the previous sections, the common conception of QON stochastization is confirmed by the direct observations of chaotic regimes during the process of simulation of heavy-ion reactions. The time-dependent Hartree–Fock calculations for head-on collisions ${}^4\text{He} + {}^{14}\text{C}$, ${}^{12}\text{C} + {}^{12}\text{C}(0^+)$, ${}^4\text{He} + {}^{20}\text{Ne}$ have been performed by Umar et al. [11] at bombarding energies near the Coulomb barrier. The results are interpreted in the term of their classical behavior. After the initial contact, a compound nuclear system relaxes into a configuration undergoing quasiperiodic or chaotic motion. The analysis of nuclear density multipole moments $\{M_{LI}(t), \dot{M}_{LI}(t)\}$ has been applied for classifying those motions by Poincare sections. The definitions of the moments are as follows,

$$M_{LI}(t) = \int d^3r r^L Y_{LM}(\hat{r}) \rho_I(\mathbf{r}), \quad M_{LI}(\omega) = \int dt \exp(-i\omega t) M_{LI}(t), \quad (3.69)$$

where isoscalar ($I = 0$) and isovector ($I = 1$) densities,

$$\rho_I(\mathbf{r}, t) = \begin{cases} \rho_p(\mathbf{r}, t) + \rho_n(\mathbf{r}, t), & I = 0, \\ \rho_p(\mathbf{r}, t) - \rho_n(\mathbf{r}, t), & I = 1. \end{cases} \quad (3.70)$$

As is shown in [11], Poincare section of the isoscalar quadrupole mode $\{M_{20}(t), \dot{M}_{20}(t)\}$ for the ${}^{24}\text{Mg}$ nuclear system seems to be filling most of the available phase space, and the corresponding autocorrelation function

$$C_{20}(t) = \int_{-\infty}^{\infty} \frac{d\omega}{2\pi} \exp(i\omega t) |M_{20}(\omega)|^2 \quad (3.71)$$

damps fast. These findings are evidence in favour of assumption that considered motion is closer to be stochastic rather than quasiperiodic.

4. CONCLUDING REMARKS

The current review presents a complete description of classical dynamics generated by the Hamiltonian of quadrupole oscillations along with identifications of those peculiarities of quantum dynamics which can be interpreted as QMCS.

We have pointed up an intimate connection between dynamics features and geometry of the PES. Interpretation of negative curvature of the PES as the source of the local instability allows one to correctly predict the critical energy of the transition to chaos for one-well potentials.

Particular attention has been given to the investigation of classical dynamics in the parameter region according to the PES with a few local minima. As shown, one of the main peculiarities of the many-well Hamiltonians is the existence of the mixed state: realization of diverse dynamical regimes (regular or chaotic) at one and the same energy in a different local minima. Up to now the vast majority of theoretical and numerical works have been focused on the behaviour of the so-called billiards or Hamiltonian systems with the simplest topology of the PES. However it is not enough for understanding of the real many-body systems with the complicated PES for which the mixed state is a situation of general position. That is the reason why the present review should be treated as one of the indispensable steps on the way to transition from the description of the model systems to the direct consideration of much more realistic systems.

We have numerically demonstrated that for potential with a localized unstable region (in particular, the localized region of negative Gaussian curvature) regular motion restores at a high energy, i. e., for these potentials R-C-R transition takes place.

QMCS in dynamics of QON were a major focus of our interest. We calculated a semiclassical approximation to an energy spectrum of the Hamiltonian of QON by quantization of the Birkhoff–Gustavson normal form. The variations of statistical properties of an energy spectrum in the process of R-C-R transition were studied. For the chaotic region all the analyzed statistical characteristics are seen to be in good agreement with the GOE predictions. The obtained results for regular regions are consistent with the hypothesis of the universal character of energy spectrum fluctuations. Nevertheless, for small level spacings we observed some deviations, which were probably due to a small admixture of the chaotic component.

We proved that the type of classical motion is correlated with the structure of the stationary wave functions of highly excited states in the R-C-R transition. Correlations were found both in the coordinate space (the lattice of nodal curves and the distribution of the probability density) and in the Hilbert space associated with the integrable part of Hamiltonian (the distribution of the wave functions in the oscillator basis and the entropy of individual eigenstates). Calculations with the scaled Planck constant, that make it possible to obtain wave functions with equal quantum numbers and energies corresponding to different types of classical motion, enabled us to separate unambiguously correlation effects in the structure of wave functions.

The Hamiltonian of QON was used as an example to study the shell structure destruction induced by the increase of nonintegrable perturbation which models residual nucleon-nucleon interaction. In the vicinity of the classical critical energy

it was observed multiple quasicrossings of the energy levels, a violation of the quasiperiodical energy dependence of the entropy, and an increase of the average value fluctuations of the operators used to classify the eigenstates of the integrable problem.

The optimization of the basis frequency and, as a consequence, the possibility of diagonalization matrices of higher dimension made it possible to trace the restoration of the shell structure in the transition $C-R_2$ from chaos to regularity.

The process of the wave packet tunnelling through the potential barrier is considered for the case of a finite motion. We have shown that the stringent correlation between level quasicrossings and a wave function delocalization leading to the resonant tunnelling takes place.

Let us now dwell on open problems. The issue of studying of QMCS in Hamiltonian systems with a few local minima represents almost a noninvestigated region. Account must be taken that, in addition to conceptual difficulties, construction of a spectrum and eigenfunctions in this case is a very difficult computational problem. However overcoming this technical problem promises an essential progress in our understanding of QMCS. In particular, the research of the structure of the same wave function in the mixed state for various regions of configuration space will allow us to find out more reliably QMCS, we are interesting in.

Calculation of the energy splitting ΔE due to tunneling is one of the oldest problems of quantum mechanics. By present one-dimensional case for the most part has gained already its sufficient understanding. Complications, which might not have been expected until recently, arise in the case of a multidimensional problem. The reason is that the semiclassical wave functions, which determine energy splitting, are sensitive to the nature of the classical motion. Wilkinson [105] calculated the energy splitting due to tunneling between a pair of quantum states, which corresponds to classical motion on tori in phase space. The case where both wave functions correspond to classical chaotic motion were discussed by Wilkinson and Hannay [106]. While the problem of the wave function structure for the mixed state remains to be solved. The configuration space in this situation breaks up naturally into different regions (separate local minima), in each by itself different dynamical regimes are realized. Thus, there is a need of a calculating scheme, that will enable us to use the partial information about each isolated region with the aim to obtain a solution of the full problem. We believe that the path decomposition expansion of Auerbach and Kivelson [107] will prove to be useful for solving 2D tunneling problem in the mixed state. This formalism allows one to express the full time evolution operator as a time convolution and surface integrations of products of restricted Green functions, each of which involves the sum over paths that are limited to different regions of configuration space. Even for complicated nonseparable potential the qualitative behaviour is readily inferred and quantitative solutions can be obtained from knowledge of the classical dynamics.

Recently Zaslavsky and Edelman [108, 109] considered a model of a billiard-type system, which consists of two chambers connected through a hole. One chamber has a circle-shaped scatterer inside, and the other one has a Cassini oval with a concave border. As was shown, the corresponding distribution function does not reach equilibrium even during the anomalous large time. We want to note, that the mixed state, at the energy a little exceeding saddle, can serve more realistic model for the study of anomalous kinetics.

In conclusion, it should be pointed out that an important problem concerning the role of a periodic orbit in the structure of wave functions was not considered in this study. In the semiclassical limit, a quantum state must be determined by the invariant sets formed by classical trajectories. These sets cover the total energy surface for systems that are chaotic in the classical limit. The approach in which the energy surface, as a whole, plays a dominant role is confirmed by the chaotic structure of nodal curves and by the random distribution of the probability density of the wave functions of highly excited states. However, the finding of Heller [107], who showed that wave functions can have the so-called scars corresponding to a high concentration of a probability density near unstable periodic orbits, demonstrates that such an approach is not complete. The reason for this is that, although the measure of periodic trajectories is zero, their contribution is essentially singular, in contrast to the smooth contribution from the energy surface. All these problems require a special analysis.

This work has strongly benefited from the help of M. L. Bolotina, M. I. Konchatnij, V. N. Tarasov, and V. V. Yanovsky. The work was partly supported by National Fund for Fundamental Research Grant F7/336-2001.

REFERENCES

1. Zaslavsky G. M. Chaos in Dynamical Systems. N. Y.: Harwood, 1985.
2. Chirikov B. V. // Phys. Rep. 1979. V. 52. P. 263.
3. Cvitanovic P. et al. Classical and Quantum Chaos. www.nbi.dk /ChaosBook/, 2000.
4. Lichtenberg A. J., Leiberman M. A. Regular and Stochastic Motion. N. Y.: Springer-Verlag, 1983.
5. Tabor M. Chaos and Integrability in Nonlinear Dynamics. N. Y.: John Wiley, 1989.
6. Wiggins S. Introduction to Applied Nonlinear Dynamical Systems and Chaos. N. Y.: Springer-Verlag, 1990.
7. Haake F. Quantum Signatures of Chaos. Berlin: Springer, 1991.
8. Reichl L. E. The Transition to Chaos. Berlin: Springer, 1992.
9. Gutzwiller M. Chaos in Classical and Quantum Mechanics. Berlin: Springer, 1991.
10. Williams R. D., Koonin S. E. // Nucl. Phys. A. 1982. V. 391. P. 72.
11. Umar A. S. et al. // Phys. Rev. C. 1985. V. 32. P. 172.
12. Bolotin Yu. L., Krivoshei I. V. // Yad. Fiz. 1985. V. 42. P. 53.

13. Arvieu R., Brut F., Carbonell J. // Phys. Rev. A. 1987. V. 35. P. 2389.
14. Rotter I. // FECCAY. 1988. V. 19. P. 274.
15. Bohigas O., Weidenmuller H. // Ann. Rev. Nucl. Part. Sci. 1988. V. 38. P. 421.
16. Swiatecki W. // Nucl. Phys. A. 1989. V. 488. P. 375.
17. Bolotin Yu. L. et al. // FECCAY. 1989. V. 20. P. 878.
18. Baranger M. Massachusetts Institute of Technology. Preprint, CTP 1808. 1989.
19. Milek B., Norenburg W., Rozmej P. // Z. Phys. A. 1989. V. 334. P. 233.
20. Weidenmuller H. // Nucl. Phys. A. 1990. V. 520. P. 509.
21. Alhassid Y., Whelan N. // Phys. Rev. C. 1991. V. 43. P. 2637.
22. Zelevinsky V. G. // Nucl. Phys. A. 1994. V. 570. P. 411.
23. Bolotin Yu. L. et al. // Yad. Fiz. 1990. V. 52. P. 669.
24. Bjornholm S. // Nucl. Phys. A. 1985. V. 447. P. 117.
25. Quantum Chaos and Statistical Nuclear Physics / Eds. T. H. Seligman, H. Nishioka. Heidelberg: Springer, 1986.
26. Blumel R., Smilansky U. // Phys. Rev. Lett. 1988. V. 60. P. 477.
27. Bolotin Yu. et al. // Yad. Fiz. 1989. V. 50. P. 1563.
28. Manfredi V. R., Salasnich L. // Intern. J. of Mod. Phys. E. 1995. V. 4. P. 625.
29. Manfredi V. R. et al. // Intern. J. of Mod. Phys. E. 1996. V. 5. P. 521.
30. Drozd S. et al. // Phys. Rev. C. 1995. V. 51. P. 2630.
31. Srokowski T., Szczurek A., Drozd S. // Phys. Rev. C. 1990. V. 41. P. 2159.
32. Mosel V., Greiner W. // Z. Phys. 1968. V. 217. P. 256.
33. Bartz B. I. et al. Metod Hartri-Foka v teorii yadra. Kiev: Naukova dumka, 1982.
34. Tabor M. // Adv. Chem. Phys. 1981. V. 46. P. 73.
35. Dubrovin B. A., Novikov S. P., Fomenko A. T. Sovremennaya Geometriya. M.: Nauka, 1985.
36. Balazs N. L., Voros S. // Phys. Rep. 1986. V. 143. P. 109.
37. Toda M. // Phys. Lett. A. 1974. V. 48. P. 335.
38. Brumer P. // Adv. Chem. Phys. 1981. V. 47. P. 201.
39. Chirikov B. V. // Atom. Energy. 1959. V. 6. P. 630.
40. Doviell P., Escande D., Codacconi J. // Phys. Rev. Lett. 1983. V. 49. P. 1879.
41. Eizenberg J., Grainer W. Microscopic Theory of the Nucleus. Amsterdam; London: North-Holland, 1976.
42. Arnold V. I., Avez A. Ergodic Problems of Classical Mechanics. N. Y.: Benjamin, 1968.
43. Mozer J. Stable and Random Motion in Dynamical Systems. New Jersey: Princeton, 1973.
44. Bolotin Yu. L., Gonchar V. Yu., Inopin E. V. // Yad. Fiz. 1987. V. 45. P. 351.
45. Bolotin Yu. et al. // Him. Fiz. 1987. V. 6. P. 1521.
46. Gilmore R. Catastrophe Theory for Scientists and Engineers. N. Y.: John Wiley, 1981.
47. Jensen R. V. // Phys. Rev. A. 1984. V. 30. P. 386.
48. Lin W. A., Reichl L. E. // Physica D. 1986. V. 19. P. 145.

49. Bolotin Yu. L., Gonchar V. Yu., Granovsky M. Ya. // JETP Lett. 1994. V. 59. P. 51.
50. Bolotin Yu. L., Gonchar V. Yu., Granovsky M. Ya. // Physica D. 1995. V. 86. P. 500.
51. Landau L. D., Lifshitz E. M. Mechanics. London: Pergamon, 1980.
52. Berry M. Chaos and Quantum Physics. Les Houches LII / Ed. M. Giannoni, A. Voros, J. Zinn-Justin. Amsterdam: North-Holland, 1991.
53. Eckardt B. // Phys. Rep. 1988. V. 163. P. 205.
54. Bohigas O., Tomsovic S., Ulmo D. // Phys. Rep. 1993. V. 223. P. 43.
55. Elyutin P. V. // Usp. Fiz. Nauk. 1988. V. 155. P. 397.
56. Bolotin Yu. L., Gonchar V. Yu., Tarasov V. N. // Yad. Fiz. 1995. V. 58. P. 1590.
57. Weissman Y., Yortner J. // Chem. Phys. 1982. V. 77. P. 1469.
58. Feit M. D., Fleck J. A., Steiger A. // J. Comp. Phys. 1982. V. 47. P. 412.
59. Feit M. D., Fleck J. A. // J. Opt. Soc. Amer. 1981. V. 17. P. 1361.
60. Fleck J. A., Morris J. R., Feit M. D. // Appl. Phys. 1976. V. 10. P. 129.
61. Chekanov N. A. // Yad. Fiz. 1989. V. 50. P. 344.
62. Chekanov N. et al. JINR Preprint E4-90-565. Dubna, 1990.
63. Birkhoff G. D. Dynamical Systems. N. Y.: Amer. Math. Soc., 1966.
64. Gustavson F. G. // Astron. J. 1966. V. 71. P. 670.
65. Brody T. A. et al. // Rev. Mod. Phys. 1981. V. 53. P. 385.
66. Landau L. D., Lifshitz E. M. Quantum Mechanics. N. Y.: Pergamon, 1977.
67. Statistical Theory of Spectra / Ed. C. E. Porter. N. Y.: Academic, 1965.
68. Bohigas O., Giannoni M., Shmit C. // Phys. Rev. Lett. 1983. V. 52. P. 1.
69. Seligman T., Verbaarschot J., Zirnbauer M. // Phys. Rev. Lett. 1984. V. 53. P. 215.
70. Bohigas O., Hag R. V., Pandey A. // Phys. Rev. Lett. 1985. V. 54. P. 645.
71. Delande D., Gray J. // Phys. Rev. Lett. 1986. V. 57. P. 2006.
72. Berry M., Tabor M. // Proc. Roy. Soc. A. 1977. V. 356. P. 375.
73. Berry M., Robnik M. // J. Phys. A: Math. Gen. 1984. V. 17. P. 2413.
74. Izrailev F. M. // Phys. Rep. 1990. V. 196. P. 299.
75. Dyson F. J., Mehta M. L. // J. Math. Phys. 1963. V. 4. P. 701.
76. Bogomolny E. B. // JETP Lett. 1985. V. 41. P. 55.
77. Wong S. S. Chaotic Behaviour in Quantum Systems / Ed. G. Casati. N. Y.: Plenum Press, 1985.
78. Bolotin Yu. et al. // Phys. Lett. A. 1989. V. 135. P. 29.
79. Ersin Y. // Phys. Rev. A. 1988. V. 38. P. 1027.
80. Meredith D. C., Koonin S. E., Zirnbauer M. R. // Ibid. V. 37. P. 3499.
81. Lipkin H. J., Meshkov N., Glick A. J. // Nucl. Phys. 1965. V. 62. P. 188.
82. Wigner E. P. // Phys. Rev. 1932. V. 32. P. 749.
83. Berry M. V. // J. Phys. A: Math. Gen. 1977. V. 10. P. 2083.
84. McDonald S. W., Kaufman A. N. // Phys. Rev. A. 1988. V. 37. P. 3067.
85. Bolotin Yu. et al. // Phys. Lett. A. 1990. V. 144. P. 459.

86. Bolotin Yu. L., Gonchar V. Yu., Tarasov V. N. // *Yad. Phys.* 1995. V. 58. P. 1499.
87. Stratt R. M., Handy C. N., Miller W. N. // *J. Chem. Phys.* 1979. V. 71. P. 3311.
88. Nordholm K. S. J., Rice S. A. // *J. Chem. Phys.* 1974. V. 61. P. 203.
89. Keller J., Rubinov S. // *Ann. Phys.* 1960. V. 9. P. 24.
90. Persival I. S. // *Adv. Chem. Phys.* 1977. V. 36. P. 1.
91. Yonezawa F. // *J. Non-Cryst. Solids*. 1980. V. 35. P. 26.
92. Reichl L. E. // *Europhys. Lett.* 1988. V. 6. P. 669.
93. Berry M. V., Wilkinson M. // *Proc. Roy. Soc. A.* 1984. V. 392. P. 15.
94. Eizenberg J., Grainer W. *Nuclear Theory*. Amsterdam: North-Holland, 1970. V. 1.
95. Takahachi K. // *Prog. Theor. Phys. Suppl.* 1989. V. 98. P. 109.
96. Zak J. // *Phys. Rev.* 1969. V. 177. P. 1151.
97. Glauber R. J. // *Phys. Rev.* 1963. V. 131. P. 2766.
98. Weissman J., Jortner J. // *J. Chem. Phys.* 1982. V. 77. P. 1486.
99. Prugovecki E. // *Ann. Phys.* 1978. V. 110. P. 102.
100. Ben-Tal N., Moiseev N. // *J. Phys. A: Math. Gen.* 1991. V. 24. P. 3593.
101. Bolotin Yu. L., Gonchar V. Yu., Tarasov V. N. // *Ukr. Fiz. J.* 1993. V. 38. P. 513.
102. Razavy M., Pimpale A. // *Phys. Rep.* 1988. V. 168. P. 307.
103. Nieto M. *et al.* // *Phys. Lett. B.* 1985. V. 163. P. 336.
104. Casati G. *et al.* *Stochastic Behavior in Classical and Quantum Hamiltonian Systems*. Berlin: Springer-Verlag, 1979.
105. Wilkinson M. // *Physica D.* 1986. V. 21. P. 341.
106. Wilkinson M., Hannay J. N. // *Physica. D.* 1987. V. 27. P. 201.
107. Auerbach M. E., Kivelson S. // *Nucl. Phys. B.* 1985. V. 257. P. 799.
108. Zaslavsky G. M. // *Chaos.* 1995. V. 5(4). P. 653.
109. Zaslavsky G. M., Edelman M. // *Phys. Rev. E.* 1997. V. 56. P. 5310.
110. Heller E. // *Phys. Rev. Lett.* 1984. V. 53. P. 1515.